LBNL-47146

ERNEST ORLANDO LAWRENCE BERKELEY NATIONAL LABORATORY

Quantum and Semiclassical Approaches to Chemical Reaction Dynamics

David E. Skinner

Chemical Sciences Division

May 2000

Ph.D. Thesis

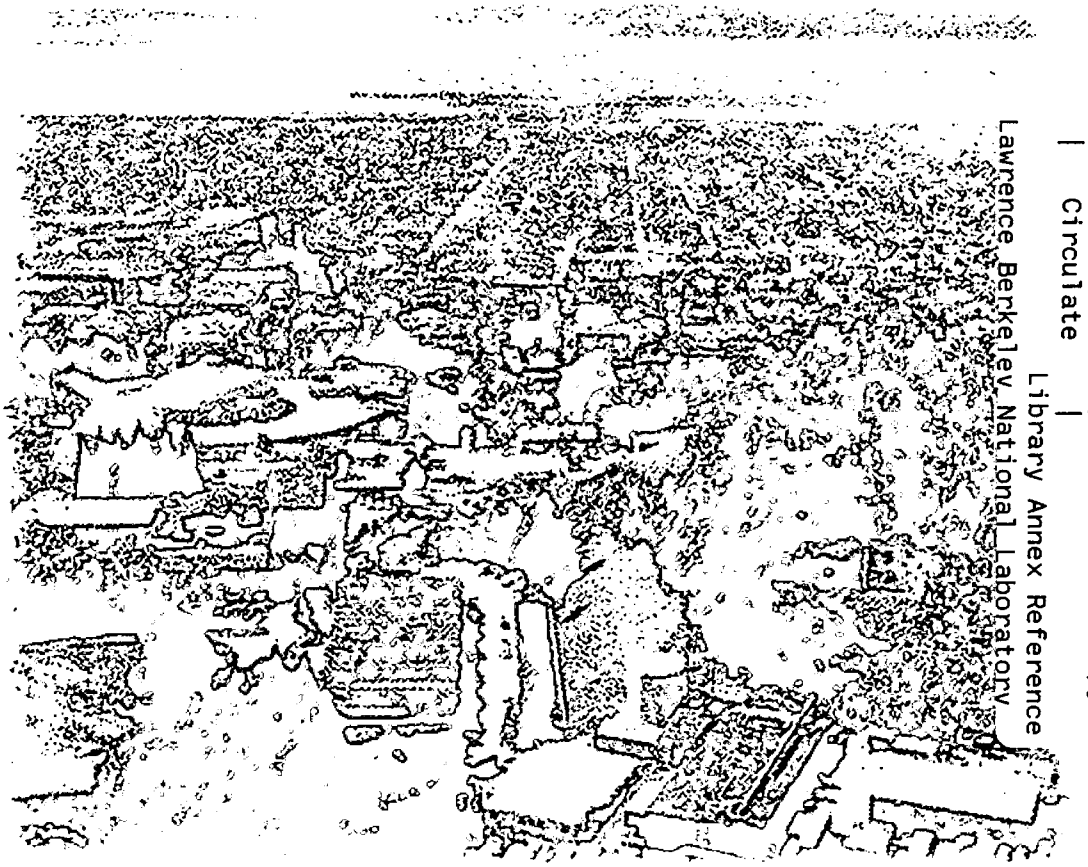

REFERENCE COPY
Does Not
Circulate

Library Annex Reference
Lawrence Berkeley National Laboratory

LBNL-47146
Copy 1

DISCLAIMER

This document was prepared as an account of work sponsored by the United States Government. While this document is believed to contain correct information, neither the United States Government nor any agency thereof, nor the Regents of the University of California, nor any of their employees, makes any warranty, express or implied, or assumes any legal responsibility for the accuracy, completeness, or usefulness of any information, apparatus, product, or process disclosed, or represents that its use would not infringe privately owned rights. Reference herein to any specific commercial product, process, or service by its trade name, trademark, manufacturer, or otherwise, does not necessarily constitute or imply its endorsement, recommendation, or favoring by the United States Government or any agency thereof, or the Regents of the University of California. The views and opinions of authors expressed herein do not necessarily state or reflect those of the United States Government or any agency thereof or the Regents of the University of California.

LBNL-47146

Quantum and Semiclassical Approaches to Chemical Reaction Dynamics

David Eugene Skinner
Ph.D. Thesis

Department of Chemistry
University of California, Berkeley

and

Chemical Sciences Division
Ernest Orlando Lawrence Berkeley National Laboratory
University of California
Berkeley, CA 94720

May 2000

This work was supported by the Director, Office of Science, Office of Basic Energy Sciences, Chemical Sciences Division of the U.S. Department of Energy under Contract No. DE-AC03 76SF00098, Lawrence Berkeley National Laboratory, and also by the National Science Foundation under Grant No. CHE97-32758.

Quantum and Semiclassical Approaches to Chemical Reaction Dynamics

by

David Eugene Skinner

B. S. (University of Kansas) 1995

A dissertation submitted in partial satisfaction of the
requirements for the degree of
Doctor of Philosophy
in
Chemistry
in the
GRADUATE DIVISION
of the
UNIVERSITY of CALIFORNIA at BERKELEY

Committee in charge:

Professor William H. Miller, Chair
Professor Robert A. Harris
Professor Robert G. Littlejohn

2000

Quantum and Semiclassical Approaches to Chemical Reaction Dynamics

Copyright ©2000

by

David Eugene Skinner

The U.S. Department of Energy has the right to use this document
for any purpose whatsoever including the right to reproduce
all or any part thereof.

Abstract

Quantum and Semiclassical Approaches to Chemical Reaction Dynamics

by
David Eugene Skinner

Doctor of Philosophy in Chemistry
University of California at Berkeley
Professor William H. Miller, Chair

In this work, we present methods for studying the dynamics of molecules as they undergo chemical reaction. Methods and applications are presented using two approaches. The first is fully quantum mechanical and as such fully accurate. The second is a semiclassical approach motivated by classical approximations to quantum mechanics.

Within both of these areas one can always extend the utility of the methods by looking for sensible approximations which faithfully represent the chemical dynamics while requiring less effort. A large portion of the present work is devoted to examination and evaluation of such economizing approximations.

In the quantum approach, we examine approximate treatments of angular momentum in the calculation of thermal rate constants. In particular we calculate thermal rates for the reaction $O + OH \rightleftharpoons H + O_2$.

In the semiclassical approach we present several methods aimed at the Monte Carlo evaluation of certain phase space integrals which arise from classical approximations to the Feynman path integral. In these methods quantum dynamics is represented

approximately via the interference of many classical trajectories. Here we will examine molecular energy transfer.

Contents

Table of Contents iv

List of Figures vi

List of Tables vii

1 Introduction 1

2 Quantum Approaches 5
- 2.1 Introduction 5
- 2.2 Reactive Flux Correlation Formalism 5
- 2.3 Quantum Dynamics on Grids 8

3 Applications to $O + OH \rightarrow H + O_2$ 14
- 3.1 Introduction 14
- 3.2 Summary of the Rate Constant Calculation 16
  - 3.2.1 General Theory 16
  - 3.2.2 Computational Specifics 19
- 3.3 Approximate Treatments for $J > 0$ 27
  - 3.3.1 The Helicity Conserving Approximation 27
  - 3.3.2 The J-shifting Approximation 29
  - 3.3.3 Principal Axis Helicty Conserving Approximation 31
  - 3.3.4 Some Further Thoughts on $J > 0$ Approximations 33
- 3.4 Results and Discussion 35

4 Semiclassical Approaches 39
- 4.1 Semiclassical Initial Value Representation 39
- 4.2 Theoretical Development 40

5 Semiclassical Molecular Energy Transfer 43
- 5.1 Introduction 43
- 5.2 LSC-IVR for the S-matrix 43

5.3 Inelastic Scattering in $He + H_2(v_i) \rightarrow He + H_2(v_f)$ 47
5.4 LSC-IVR Results 53
5.5 Molecular Energy Transfer via FB-IVR 54
5.5.1 Probability Distribution of Molecular Energy Transfer 57
5.5.2 Translation Energy Distribution 61
5.6 Application to $He + H_2(v_i) \rightarrow He + H_2(v_f)$ 63
5.7 FB-IVR Results 64
5.8 FB-IVR for Larger Systems 71

6 Summary and Conclusions **75**

References **78**

List of Figures

1.1 From small systems to large systems 3

2.1 Flux Correlation Methods 7
2.2 A Schematic Reactive Flux Correlation Function 9
2.3 The Sinc Function DVR Basis 12
2.4 Sparse Matrix Multiplication 13

3.1 HO_2 thermal flux eigenvalues at 600K and 1000K 18
3.2 Contour plot of the HO_2 DMBE IV potential energy surface 20
3.3 The Jacobi coordinates for the molecular system. 21
3.4 (J, K) dependence of the thermal flux eigenvalues at 600K 22
3.5 J selected flux correlation functions (T = 600K) 23
3.6 J selected thermal rates 24
3.7 Total Thermal Rates for $H + O_2 \rightarrow O + OH$ 25

5.1 The Secrest-Johnson surface for inelastic scattering 48
5.2 SC-IVR vibrational transition probabilities ($E = 8.0$) 49
5.3 SC-IVR vibrational transition probabilities (E=12) 50
5.4 Comparison of Linearized and SC-IVR vibrational transition probabilities (E=12) 51
5.5 Comparison of Linearized and SC-IVR vibrational transition probabilities (E=12) 52
5.6 Comparison of Quantum and FB-IVR Correlation Functions 65
5.7 Energy Transfer Spectra (E=8.0) 66
5.8 Energy Transfer Spectra (E=12.0) 67
5.9 FB-IVR vibrational transition probabilities ($E = 8.0$) 68
5.10 FB-IVR vibrational transition probabilities ($E = 12.0$) 69

List of Tables

3.1 Rotational Constants and Partition Functions at Fixed Geometries. . 37
3.2 Parameters Describing the Dependence of $k_{JK}(T)$ on J and K in Equation(3.30) 37
3.3 Thermal Rate Constants for $H + O_2 \rightarrow O + OH$ 38

5.1 Molecular Energy Transfer Probabilities for $H_2(\nu) + He \rightarrow H_2(v') + He$ $(E = 8.0)$ 73
5.2 Molecular Energy Transfer Probabilities for $H_2(\nu) + He \rightarrow H_2(v') + He$ $(E = 12.0)$ 74

Acknowledgements

It has been a great joy to conduct research with Professor Miller the past five years. I have learned from him, among many things, a completely new way to think about chemical reactions than I had before coming to Berkeley. Professor Miller is both a fountain of great ideas and an excellent advisor to his students. Many times have I walked into his office confused and exited enlightened.

My kind thanks go to Cheryn Gliebe for making my graduate experience a pleasant one and for gently reminding me to enroll from time to time. You really do an amazing job for the group.

I would like to thank the entire Miller group, past and present, with whom I have had many productive collaborations and entertaining blackboard talks. The concentration of great ideas in the group and at Berkeley in general has made studying here tremendously rewarding.

I am particularly indebted to Ward Thompson for many discussions regarding quantum mechanics and reaction rates. I am grateful for Chris Maierle's kind friendship and many wonderful hours of scientific discussion.

By far the best coursework I have ever taken was during my early years at Berkeley. My classes with Professor Miller, Professor Harris, Professor Littlejohn, and Professor Neu prepared me for the research described in this thesis. My notes from these classes are invaluable to me, as is the experience gained in my teaching assitantship with professor Miller.

This thesis and indeed my entire graduate education would not have been possible without all the great teachers I had before coming to Berkeley. Thank you Dave Webb, Susan Miller, Bob Sander, Andrew Bennett, Bob Bowman and Bill Paschke for your teaching, time, and encouragement.

I also wish to thank the Fannie and John Hertz Foundation for the fellowship which kindly funded my education at Berkeley.

This work has been supported by the Director, Office of Science, Office of Basic Energy Sciences, Chemical Sciences Division of the U.S. Department of Energy under contract No. DE-AC03 76SF00098, Lawrence Berkeley Na-

tional Laboratory, and also by the National Science Foundation under Grant No. CHE97-32758.

Chapter 1

Introduction

Chemical reaction dynamics is the study of the motions molecules make during the course of a chemical reaction. By understanding these movements we can determine how chemical change occurs and may also calculate many physically useful quantities. In the present work we are primarily interested in the rates of chemical reaction, but a dynamical understanding of the reaction allows further insight as to the energetics and mechanism involved. Indeed, a fully dynamical account of a chemical reaction allows any and all molecular change to be studied in detail. We will examine methods that fall short, on purpose, of a complete description of chemical change, but provide detailed answers to specific questions. Such an appropriately detailed understanding of chemical reactions is the goal of the work presented here.

The central statement of the dynamics of molecules at the quantum mechanical level is the time dependent Schrodinger equation. In a simplistic sense the enterprise of chemical physics must only implement an already known theory, quantum mechanics, for chemical systems. No new theories need be developed. We must simply write down a known Hamiltonian for the molecular system and solve the time dependent Schrodinger equation,

$$i\hbar\frac{d}{dt}|\psi(t)\rangle = \hat{H}|\psi(t)\rangle, \tag{1.1}$$

for $|\psi(t)\rangle$, from the initial wave function $|\psi(0)\rangle$. From $|\psi(t)\rangle$, all physical properties

of the system are directly available. This approach, while quite general, suffers on two accounts.

The first reason is that the application of basis set methods to Equation (1.1) for chemical problems, particularly problems involving chemical reactions, quickly becomes computationally intractable as the molecules approach sizes common to chemistry (CH_4, Amino Acids, and larger). The size of the direct product basis set needed is $\sim N^d$, where N is the number of basis functions needed for each degree of freedom d. The exponential scaling of basis size with dimensionality presents a bottleneck in terms of the memory required to complete the calculation on a computer. Currently, a memory size on the order of a gigabyte is typical to most workstations. Assuming, optimistically, that we need 10 basis function per degree of freedom we can approach a 5 dimensional problem, but larger problems will always lie increasingly out of reach.

Even if we could accomplish the calculation, what would we do with the solution $|\psi(t)\rangle$? Often we are interested in a *specific* physical property of the system (as opposed to complete knowledge), and the calculation of that property will nearly always involving throwing away information contained in the complete $|\psi(t)\rangle$. For instance to calculate a thermal reaction rate we would time evolve reactant states, by solving Equation(1.1), and project on to product states in order to determine the amplitude,

$$S_{n_p,n_r}(E) = -\frac{i}{\hbar}\langle\psi_{n_p}|\hat{\epsilon}_p\hat{G}(E)\hat{\epsilon}_r|\psi_{n_r}\rangle \tag{1.2}$$

where $\hat{G}(E)$ is the Green's function and n_r and n_p are respectively the reactant and product quantum numbers. The thermal rate collapses all of this information via,

$$k(T) = [2\pi\hbar Q_r(T)]^{-1}\int_{-\infty}^{\infty} dE e^{-E/kT}\sum_{n_p,n_r}|S_{n_p,n_r}(E)|^2 \tag{1.3}$$

into a single number. In chapter 2 we will present ways around this by using alternative methods for the efficient calculation of $k(T)$ directly.

The second problem with pursuing the direct solution via Equation(1.1) has to do with the *size* of molecules. Molecules inhabit the boundary world between quantum and classical physics. The atomic constituents of molecules span the range of masses from $\sim 10^{-24}$ to 10^{-22} grams, and even within this low mass range, the impact of

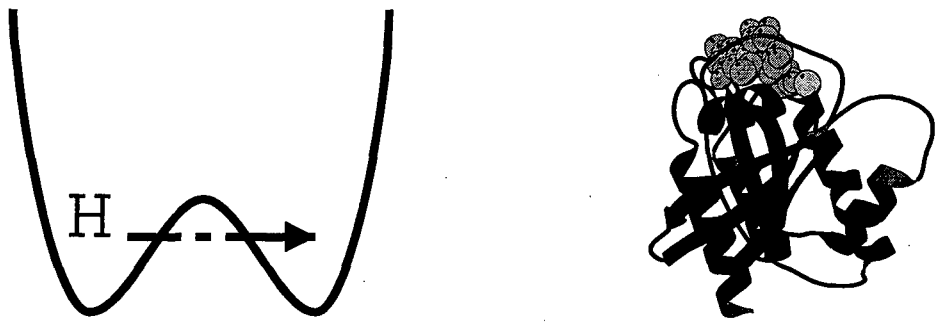

Figure 1.1: The range of chemical systems spans the range from motion of individual protons through chemical barriers to the dynamics of large protein structures.

quantum mechanical phenomena varies greatly. The chemical region beyond few atom systems *e.g.*proteins, can involve many millions of molecular constituents.

It is important to ask what impact we expect quantum mechanics to have on systems as they become larger. For the fast vibration or translation of a low mass particle such as an H atom we would expect that tunneling and interference actively contribute to the dynamics. Indeed these processes play a significant part in proton transfer, the dynamics of delocalized states, and electronically non-adiabatic processes. In this regime the use of fully quantum dynamics is appropriate and quite likely necessary.

Consider on the other hand the dynamics of a protein whose slowly swaying molecular framework may approach that of classical dynamics due to the great masses involved. For this type of motion, quantum effects will manifest themselves, if at all, only in more subtle ways. For this reason, classical molecular dynamics has been quite successful in exploring chemical dynamics in this regime. Indeed, molecular dyanamics based on classical dynamics is widely used througout chemistry, materials science, and biology. Since the solution of classical dynamics is trivial compared to the effort needed for a quantum solution we would much prefer to utilize, when possible, a description of molecular dynamics which is motivated by this simpler classical motion. Chapter 4 presents the theory of such semiclassical methods.

Given that the theory that fully describes chemical dynamics is not one we can

apply directly to systems of chemical interest, the real work of chemical dynamics is the discovery of approaches which can either reduce the effort of computation by calculating reduced quantities directly or by leveraging the near-classical behavior of chemical sized systems to provide approximate descriptions of chemical dynamics based in quantum mechanics. It is from these methods that a physical understanding of processes at a truly molecular level can be developed.

The body of this work is divided into four main sections. In chapters 2 and 4 we present background on the theory and ideas behind the quantum and semiclassical approaches. In chapters 3 and 5 we implement these theories by studying specific chemical systems. Summary and conclusions are presented in chapter 6.

Chapter 2

Quantum Approaches

2.1 Introduction

In this chapter we will present background on the theories that will be implemented in the next chapter. The focus of the methods in on calculating thermal rates, $k(T)$, in a rigorous way quantum mechanically. A necessary part of this calculation, and indeed the most time consuming, is evolving wave functions in time. Therefore, a discussion of computer implementations of quantum dynamics is also presented.

2.2 Reactive Flux Correlation Formalism

The direct quantum approach to the thermal rate presented in Equation(1.3) of the last chapter is quite inefficient since it generates a large amount of detailed information which is then combined to provide the rate constant. Miller[1] has shown that the thermal reaction rate constant, $k(T)$ may be expressed more efficiently and directly as:

$$\begin{aligned} k(T) &= \frac{1}{Q_r}\int_0^\infty C_{rp}(t)dt \\ C_{rp}(t) &= \mathrm{tr}[e^{-\beta\hat{H}/2\hbar}\hat{F}_r(0)e^{-\beta\hat{H}/2\hbar}\hat{F}_p(t)] \end{aligned} \tag{2.1}$$

Where $\hat{F}_r(0)$ and $\hat{F}_p(t)$ are the Heisenberg evolved flux operators for dividing

surfaces defining product ($\hat{F}_p$) and reactant ($\hat{F}_r$) regions of the potential energy surface (PES). Each flux operator is defined in relation to a surface through the coordinate space. We can think of such a surface as a Heaviside operator, $\hat{h}$ and write the flux operator as,

$$\hat{F} = \frac{d}{dt}\hat{h} = \frac{i}{\hbar}[\hat{H}, \hat{h}]. \tag{2.2}$$

We define the thermal flux operator,

$$\hat{F}(\beta) = e^{-\beta\hat{H}/2\hbar}\hat{F}_r(0)e^{-\beta\hat{H}/2\hbar}, \tag{2.3}$$

which is simply a flux operator Heisenberg evolved to the imaginary time $t_\beta = -i\beta/2\hbar$. The other flux operator appearing in Equation(2.1) is likewise the real time evolved $\hat{F}(t)$.

Efficient evaluation of $k(T)$ via equation(2.1) depends on choosing an appropriate basis for evaluating the trace. One convenient set of basis functions are the eigenkets of the thermal flux operator $\hat{F}(\beta)$

$$\hat{F}(\beta)|\psi_i >= \lambda_i|\psi_i > \tag{2.4}$$

Evaluating the trace in equation (2.1) in this basis gives the rate as:

$$k(T) = \frac{1}{Q_r}\sum_i \lambda_i \int_0^\infty < \psi_i|\hat{F}(t)|\psi_i > dt \tag{2.5}$$

Since the thermal flux operator may be shown to be of low rank, the sum may be restricted to only those λ_i which are large enough to contribute to the rate. This is the primary benefit of the present method. The low rank property means that a minimum of wave functions will need to be propagated. The number of thermal flux eigenfunctions that will be needed to evaluate the trace in Equation (2.1) is analogous to the number of states at the transition state. In the next chapter we will see a further demonstration of the low rank property in the application of this theory to a particular chemical system.

$< \psi_i|\hat{F}(t)|\psi_i >$ is calculated by propagating the thermal flux eigenfunctions on the PES with an absorbing potential at the boundary to properly treat the boundary

Rate Constants from Flux Correlation Functions

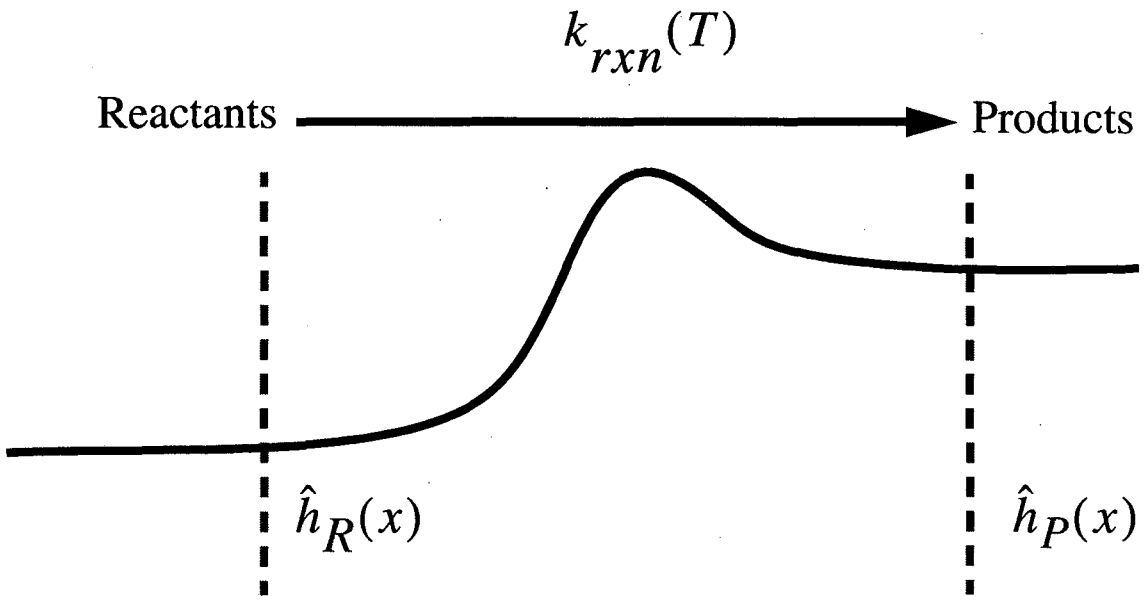

$$k_{rxn}(T) = Q_R^{-1} \int_0^\infty tr\left[e^{-\beta \hat{H}} \hat{F}_R e^{i\hat{H}t} \hat{F}_P e^{-i\hat{H}t}\right] dt$$

$$= Q_R^{-1} \int_0^\infty \langle \hat{F}_R(0) \hat{F}_P(t) \rangle_{therm} dt$$

Figure 2.1: Flux Correlation Methods

conditions. The absorbing potential is negative imaginary term added to the Hamiltonian which damps the wave function in a particular region. When carefully applied the absorbing potential enforces the boundary conditions by allowing asymptotic flux to permanently leave the reaction region. Absorbing potentials would typically be placed in the asymptotic product channels in order to properly enforce the boundary conditions.

The thermal flux eigenfunction is localized at the flux dividing surface at $t = 0$. As the wavefunction is propagated in time, flux crosses both reactant and product dividing surfaces. Flux crossing the surface towards products contributes positively to the correlation function and to the rate. Recrossing flux contributes negatively to the rate. The correlation functions $C_{rr}(t)$ and $C_{rp}(t)$ track this flux as the reaction proceeds. A schematic example of a flux correlation function is shown in Figure (2.2). The transition state theory approach misses this recrossing flux and thus over estimates the rate constant.

In order to carry out a calculation of $k(T)$ using this method we still must be able to propagate the wave functions in both real and imaginary time. This will be the largest computational task involved in the determination of the reaction rate.

2.3 Quantum Dynamics on Grids

As seen above in equation(2.5), the choice of an appropriate basis for evaluating the trace has a great impact on making the theory practical. It is likewise so for the propagation of wavefunctions. We must find a suitable basis such that the action of the time evolution operator $e^{-i\hat{H}t/\hbar}$ on an arbitrary state is computable in an efficient way. The approach we take is to express the propagator as a product of one dimensional kinetic energy operators and a potential energy factor and to find a basis which admits an simple form for these one dimensional terms.

Let us suppose that the Hamiltonian has the following two dimensional form:

$$\frac{\hat{P}_x^2}{2m} + \frac{\hat{P}_y^2}{2m} + \hat{V}(x, y). \tag{2.6}$$

For this example Hamiltonian we may expand the propagator as,

Figure 2.2: A typical reactive flux correlation function, which depicts the contribution from transition state flux as well as recrossing flux.

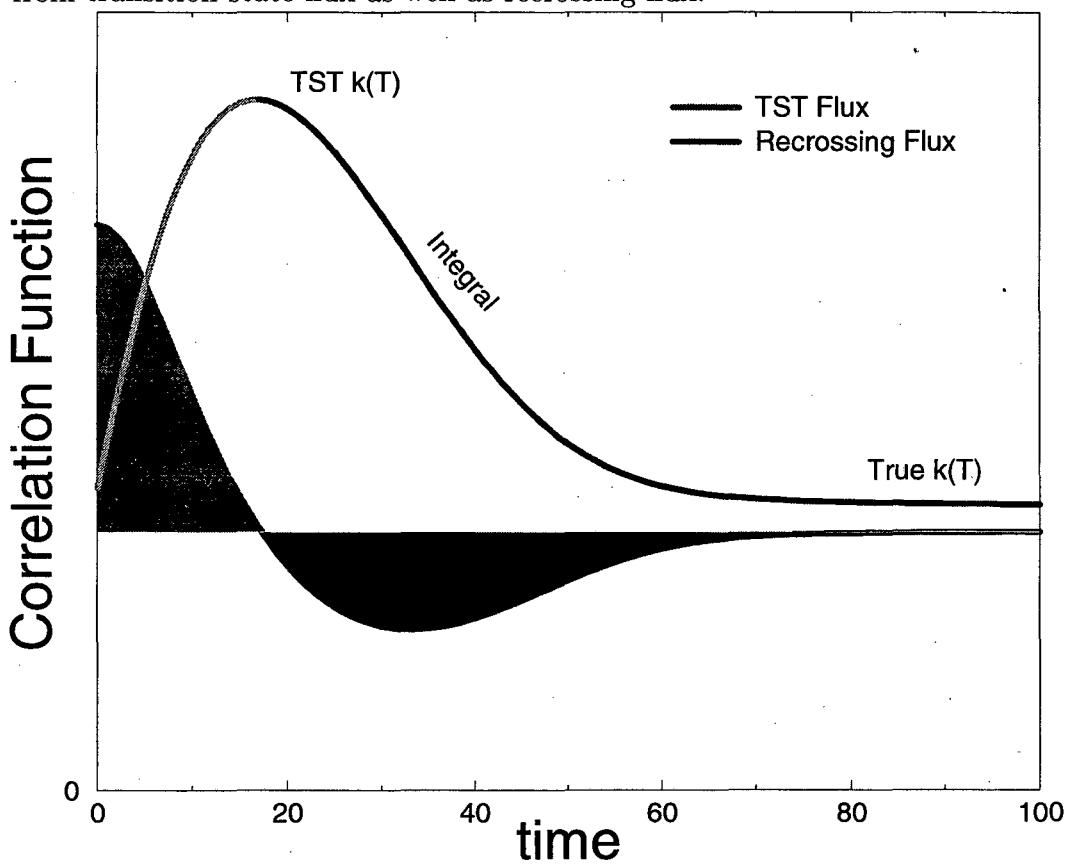

$$e^{-i\hat{H}t/\hbar} \simeq e^{-i\hat{T}_x t/2\hbar} e^{-i\hat{T}_y t/2\hbar} e^{-i\hat{V}_{xy} t/\hbar} e^{-i\hat{T}_y t/2\hbar} e^{-i\hat{T}_x t/2\hbar}. \tag{2.7}$$

Though this expansion[2] is approximate, for sufficiently small t the error is $o(t^2)$. We will assume that we always choose t small enough that this error is negligible. Similar expansions hold for other Hamiltonia, but for the present illustration a two dimensional cartesian example will do.

If we construct the direct product basis,

$$|\psi\rangle = \sum_{ij}^{N_x N_y} c_{ij} |\phi_i^x\rangle |\phi_j^y\rangle, \tag{2.8}$$

then we seek one dimensional basis sets $|\phi_i^x\rangle$ and $|\phi_j^y\rangle$ such that the matrices,

$$\langle \phi_i^x | \hat{T}_x | \phi_j^x \rangle \;\; and \;\; \langle \phi_i^y | \hat{T}_y | \phi_j^y \rangle \tag{2.9}$$

are readily computable. Several such bases exist. The Fourier functions and their bandwidth limited counterparts, the sinc functions, being among the simplest examples.

For example in the Fourier basis our kinetic energy operators have the form,

$$\hat{T} = \hat{U}_{FFT}^{\dagger} \; diag \left(\frac{-\hbar^2 (j - N_x/2)^2}{2\mu \Delta x^2} \right) \; \hat{U}_{FFT}, \tag{2.10}$$

which is easily exponentiated to give the propagator as,

$$e^{-it\hat{T}/\hbar} = \hat{U}_{FFT}^{\dagger} \; diag \left(e^{\frac{it\hbar(j-N_x/2)}{2\mu\Delta x^2}} \right) \; \hat{U}_{FFT}. \tag{2.11}$$

The Fourier basis is particularly useful in that the transformations $\hat{U}_{FFT}$ may be applied using only $N_x log N x$ multiplications in applying the matrix owing to the symmetry of these functions. A strong disadvantage of this basis is that it must be used on a regular,*i.e.* rectangular, grid. Thus the memory required to store a wave function scales exactly as the worst case N^d situation.

One way around this problem is to use a sparse grid of irregularly spaced points. This is quite natural using sinc $(sin(x)/x)$ functions,

$$|\phi_n(x)\rangle = \frac{1}{2\sqrt{\pi}\omega_{max}} \int_{-\omega_{max}}^{\omega_{max}} e^{-i\omega x} e^{in\pi\omega/\omega_{max}} d\omega \tag{2.12}$$

$$= \sqrt{\frac{\omega_{max}}{\pi}} sinc(\omega_{max} - n\pi) \tag{2.13}$$

The label n is an index for the grid coordinates $x_n = n\pi/\omega_{max}$. The sinc function DVR is further illustrated in Figure(2.3).

An important aspect of the sinc function DVR is that we may delete members of the direct product basis in unphysical regions. If, for instance, the potential energy in a particular region is so high that we expect the amplitude of the wave function to be vanishingly small, deleting the basis in that region is equivalent to imposing this assumption on the calculation. Similar constraints may be imposed with respect to the kinetic energy. For a typical chemical potential energy surface it is not unusual to be able to shrink the size of the basis to about 20% of the original number (N^d scaling).

Sparse matrices on irregular grids operate on kets in the same way as dense operators, though we need not store all the elements. An effective way of operating a sequence of one dimensional operators on such a multidimensional sparse vector is is via the reordering process shown in Figure(2.4). Before acting $e^{-it\hat{T}_x/\hbar}$ on the ket we order the vector so that the index corresponding to dimension x changes most rapidly, with the other dimensions ordered in an increasing but arbitrary order. Sorted this way contiguous sections of the fastest running index, *e.g.*x, correspond to one dimensional line segments in the multidimensional sparse grid. Acting $e^{-it\hat{T}_x/\hbar}$ on the ket is then simply a sequence of small one dimensional matrix multiplications on each segment. This method has the great computational advantage of sequential memory access and speeds up the propagation significantly.

The above tools allow one to transform a problem in chemical reaction dynamics into what is essentially a large linear algebra problem to be implemented on a computer. In the next chapter we will apply these methods to a specific example important in combustion and atmospheric chemistry.

Figure 2.3: The Sinc Function DVR Basis

$$|j> \propto \frac{sin(\pi(x/\Delta x - j))}{x/\Delta x - j}$$
$$\Delta = \pi/\omega_{max}$$

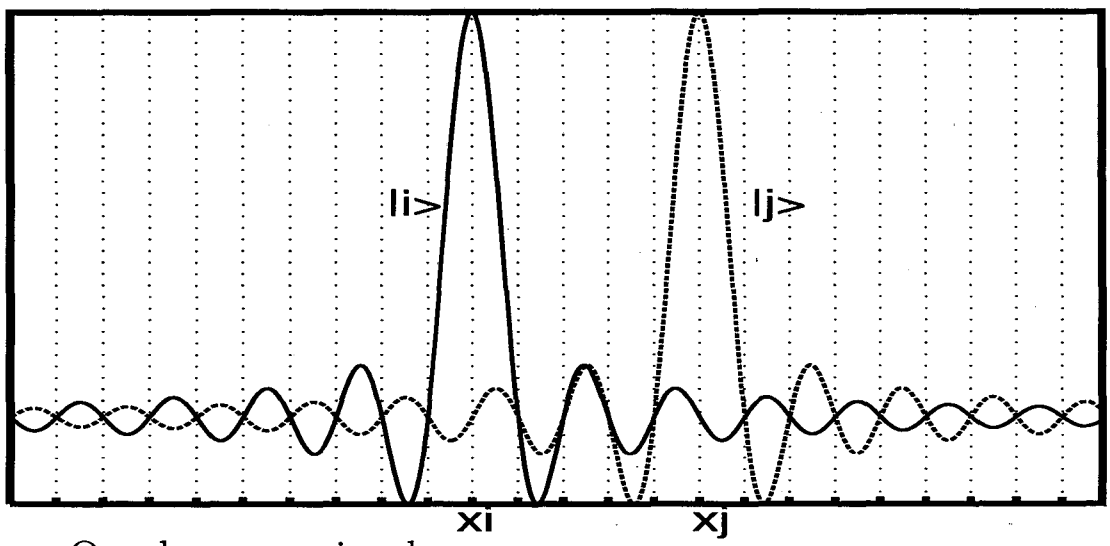

- Overlaps are simple:

$$\begin{aligned}\langle i|j\rangle &= \int_{-\infty}^{\infty} \Psi_i^\star(x)\Psi_j(x)dx \\ &\simeq \sum_{-\infty}^{\infty} \Psi_i^\star(x_i)\Psi_j(x_i)\Delta x \\ &= \delta_{ij}\end{aligned}$$

$$\langle i|\frac{\partial^k}{\partial x^k}|j\rangle = \frac{\partial^k}{\partial x^k} sinc(\frac{\pi}{\Delta}x)|_{x=(n-m)\Delta}$$

- Grid spacing determines largest representable momentum:

$$p_{max} = \hbar/\Delta x$$

- Operators are sparse

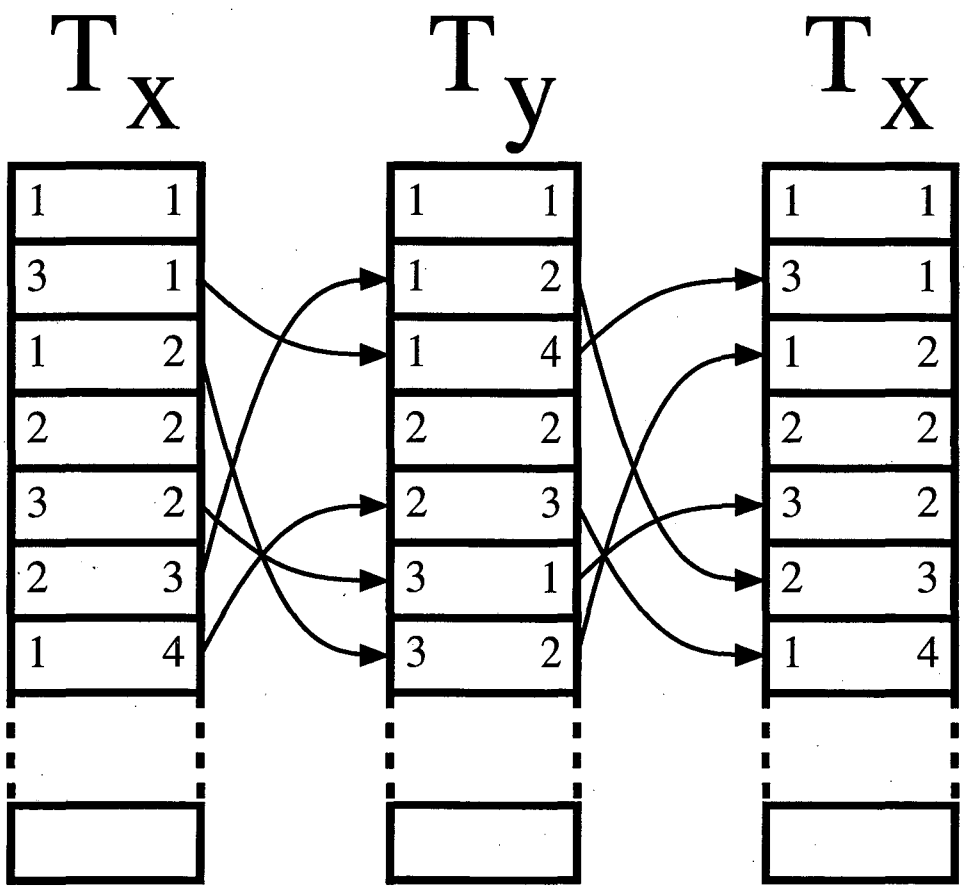

Figure 2.4: Sparse matrix multiplication where each box represents an element of the ket vector and is labeld by it's y index first and x index second. Reordering between applications of one dimensional operator increases efficiency.

Chapter 3

Applications to $O + OH \rightarrow H + O_2$

3.1 Introduction

In this chapter we apply the methods outlined in the previous chapter to the problem of angular momentum in chemical reactions. Often the basis set needed for a chemical system is so big that only the $J = 0$ part of the computation may be carried out. Here we examine methods of including the effects of angular momentum on thermal reaction rates.

A recent paper[3] presented the results of rigorous quantum mechanical calculations of the rate constant of the reaction $O + OH \rightleftharpoons H + O_2$ (and also recombination to HO_2 via collisional relaxation by a bath gas). Because of its importance in combustion and atmospheric modeling[4–7] this reaction has been the focus of many studies, *e.g.*, classical trajectory simulations[8], statistical (RRKM) rate[9] and quantum scattering calculations[10–13], and also studies of the HO_2 bound[14] and metastable states[15]. Previous calculations, however, have only carried out explicitly for zero total angular momentum ($J = 0$), the contribution to the rate constant for $J > 0$ being approximated by the "J-shifting" approximation (JSA)[16], which assumes that rotational motion is separable from the other degrees of freedom and furthermore that it is that of a rigid rotor (with some assumed geometry). The purpose of this work is to report the results of more accurate calculations for $J > 0$, to test the accuracy of the JSA and see to what extent it is reliable for this reaction. We note that there have been

some previous calculations for $J > 0$: those by Wu and Hayes[14] for bound state energy levels of HO_2 for J up to 3, and those by Meijer and Goldfield[17] for total reaction probabilities of $H + O_2(v = 0, j = 1)$ for $J = 0, 1, 2, 5$.

How to deal with the $J > 0$ contribution to the thermal rate constants is a non-trivial matter, particularly so for the present reaction which is extremely challenging even for $J = 0$ because of the existence of a long-lived collision complex. At the most rigorous level of theory the quantum mechanical calculation of the rate constant is carried out separately for each value of J, and the total rate constant is the sum of those for each J,

$$k(T) = \sum_{J=0}^{\infty} (2J + 1) k_J(T). \tag{3.1}$$

Typically many values of J contribute to this sum, the more so the higher the temperature, and the calculation for each J is more difficult than for $J = 0$ because there is an additional coupled degree of freedom. (Matters are not quite so bleak, however, because the J dependence of the $k_J(T)$ is usually very simple; one can thus perform the calculation for a few widely spaced values of J and then interpolate to evaluate the sum in Equation(3.1)[18]).

The next section first briefly summarizes the methods used to calculate the rate constant (for each J), a fully rigorous quantum mechanical approach based on reactive flux correlation methods[1,19]. We then describe the helicity conserving approximation (HCA) used for the present $J > 0$ calculations. A more general HCA is also described, one based on the instantaneous principal axes of the molecular system, and an even wider range of possible approximations for $J > 0$ calculations is also surveyed that may be useful in other applications. The results of the calculation of $k(T)$ for the present reaction are presented and used to compare the quality of the approximations considered. It is seen that the simplest, JS approximation is not so bad ($\sim 10 - 20\%$ error) for the present reaction, provided the proper choice is made for the reference geometry.

3.2 Summary of the Rate Constant Calculation

3.2.1 General Theory

Within the HCA (see section 3.3.1 below) the calculation of the rate constant for $J > 0$ is the same as that for $J = 0$ with an effective potential energy surface V_{JK} that depends parametrically on J and K, the projection of the total angular momentum onto a body-fixed axis. K (the helicity) is assumed to be conserved in the HCA, and $k_J(T)$ of Equation(3.1) is given by

$$k_J(T) = \sum_{K=-J}^{J} k_{JK}(T), \tag{3.2}$$

where $k_{JK}(T)$ is the result of the rate constant calculation with the effective potential V_{JK}.

The rate constant calculation is carried out for each value of J and K. Because the reaction proceeds via a long-lived collision complex, *i.e.*,

$$O + OH \rightleftharpoons HO_2^{\ddagger} \rightarrow H + O_2 \tag{3.3}$$

it is useful to compute the rate constant as the time integral of a *cross* correlation function rather than as a flux *auto*correlation function as has been most commonly done in other applications,

$$k(T) = Q_r(T)^{-1} \int_0^{\infty} dt\, C_{rp}(t), \tag{3.4}$$

where $Q_r(T)$ is the reactant partition function per unit volume and $C_{rp}(t)$ is given by,

$$C_{rp}(t) = tr[e^{-\beta\hat{H}/2}\hat{F}_r e^{-\beta\hat{H}/2} e^{i\hat{H}t/\hbar}\hat{F}_p e^{-i\hat{H}t/\hbar}]. \tag{3.5}$$

Here the flux operators, $\hat{F}_r$ and $\hat{F}_p$, are defined with respect to two different dividing surfaces, one on the reactant($O \cdots OH$) side of the $HO_2^{\ddagger}$ complex region and the

other on the product($H + O_2$) side, respectively; see Figure 3.2 . (For simplicity of presentation, the Hamiltonian in Equation(3.5), and elsewhere in the following sections, is not labeled by the specific (J, K) value of the calculation.)
The most efficient way we have yet developed for evaluating these flux correlation functions is that described by Thompson and Miller[20], which has been used before for the $O + HCl \rightarrow OH + Cl$[21] and $Cl + H_2 \rightarrow HCl + H$[18] reactions, as well as our earlier $J = 0$ calculations for the present reaction[3]. (One should also see the work of Light *et al.*[22] and Matzkies and Manthe[23] which has features similar to our approach.) The first step in this approach is a Lanczos iteration calculation[24] to find the relatively small number of non-zero eigenvalues λ_i and corresponding eigenvectors $|v_i\rangle$ of the Boltzmannized flux operator

$$\hat{F}_r(\beta) = e^{-\beta\hat{H}/2}\hat{F}_r e^{-\beta\hat{H}/2}, \tag{3.6a}$$

which can then be represented as

$$\hat{F}_r(\beta) = \sum_i \lambda_i |v_i\rangle\langle v_i|. \tag{3.6b}$$

The Lanczos procedure is particularly efficient because $\hat{F}_r(\beta)$ is of low rank, *i.e.*, has a small number of non-zero eigenvalues (approximately twice the number of thermally accessible states on the reactant dividing surface). Figure 3.1 shows the positive eigenvalues of $\hat{F}_r(\beta)$ for temperatures T=600 K and 1000 K, showing how the number increases with T. (The eigenvalues occur in $\pm$ pairs, with the eigenvector of the negative eigenvalue being the complex conjugate of that for the positive eigenvalue[25,26].)

The trace in Equation(3.5) is then evaluated in the basis of these eigenvectors, giving

$$k(T) = Q_r(T)^{-1} \sum_i \lambda_i \int_0^\infty dt\ \langle v_i(t)|\hat{F}|v_i(t)\rangle \tag{3.7}$$

where $|v_i(t)\rangle$ is the time evolved vector

$$|v_i(t)\rangle = e^{-i\hat{H}t/\hbar}|v_i\rangle. \tag{3.8}$$

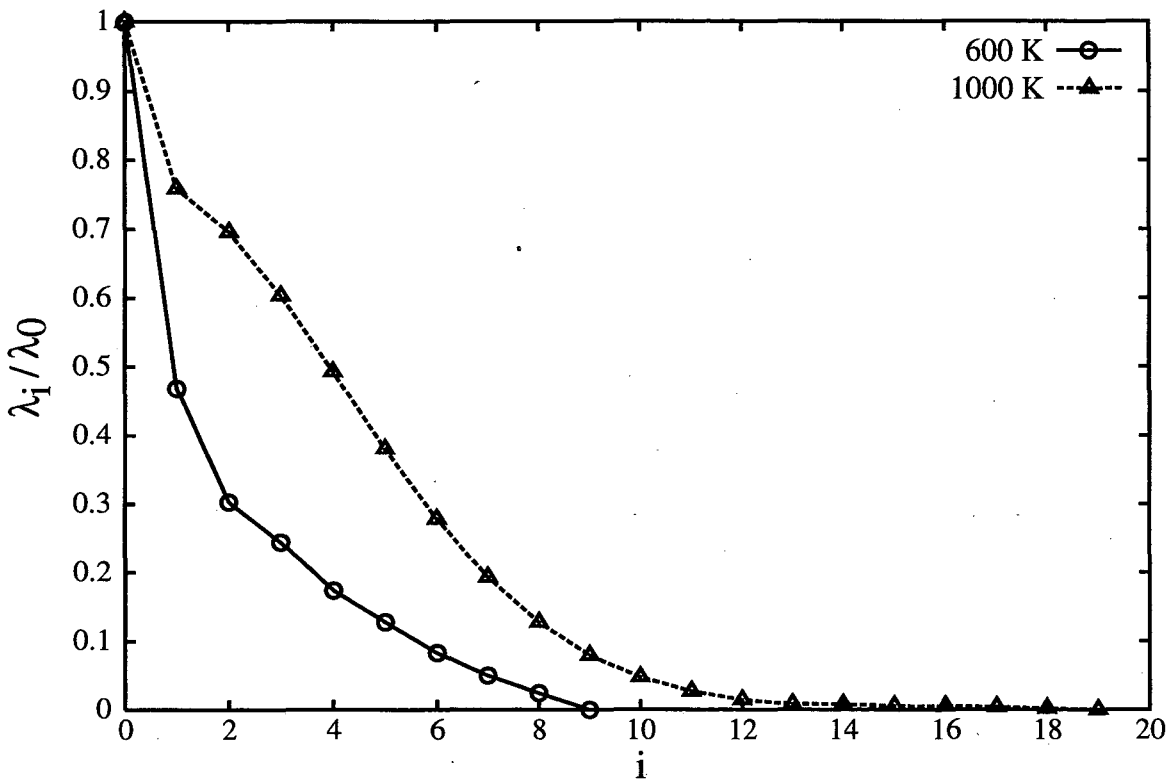

Figure 3.1: The positive thermal flux eigenvalues (λ) at 600 K and 1000 K for $J = 0$ for the dividing surface at the $O \cdots OH$ transition state. The rapid convergence to zero demonstrates the low rank of $\hat{F}_\beta$.

We used the split operator algorithm to carry out this time evolution, though other methods for wave packet propagation could also be used.

We note that the general principle in this type of calculation is to choose the dividing surface at the position for which $\hat{F}(\beta)$ will be of the lowest rank possible, so as to minimize the number of vectors which must be time evolved (Equation(3.8)). This will typically (but may not always) be the dividing surface through the highest energy transition state, *e.g.* $\hat{F}_r$ in Figure 3.2 . This feature of the procedure is very reminiscent of the variational character of transition state theory[27], where one chooses the dividing surface to minimize the number of states of the activated complex. In the present (fully dynamical) approach the final result for the rate constant is *formally* independent of where the dividing surface(s) is(are) located but the *efficiency* of the calculation is not.

3.2.2 Computational Specifics

A discrete variable representation[28] (DVR) basis was used to represent the wavefunction at a set of grid points. The underlying finite basis consists of Fourier functions in the r and R coordinates and associated Legendre functions in the γ coordinate. A basis set using $64 \times 128 \times 32$ grid points in the R, r, γ coordinates, respectively, was found to be adequate for the present calculations.

Both the thermal and real time propagation was carried out using the following split-operator[2] factorization of the full quantum propagator,

$$e^{-i(\hat{H}-i\hat{\epsilon})\Delta t} \simeq e^{-i(\hat{V}-i\hat{\epsilon})\Delta t/2} e^{-i\hat{T}_\gamma \Delta t/2} e^{-i\hat{T}_R \Delta t} e^{-i\hat{T}_r \Delta t} e^{-i\hat{T}_\gamma \Delta t/2} e^{-i(\hat{V}-i\hat{\epsilon})\Delta t/2} \tag{3.9}$$

which expresses (with $\hbar = 1$) the full propagator as a series of 1D kinetic energy operators which can be applied efficiently within the DVR formulation. In order to apply each 1D operator one transforms to a basis in which the operator is diagonal. For r and R these are Fourier transforms and for γ Legendre transforms. Denoting these transformations as unitary matrices one has,

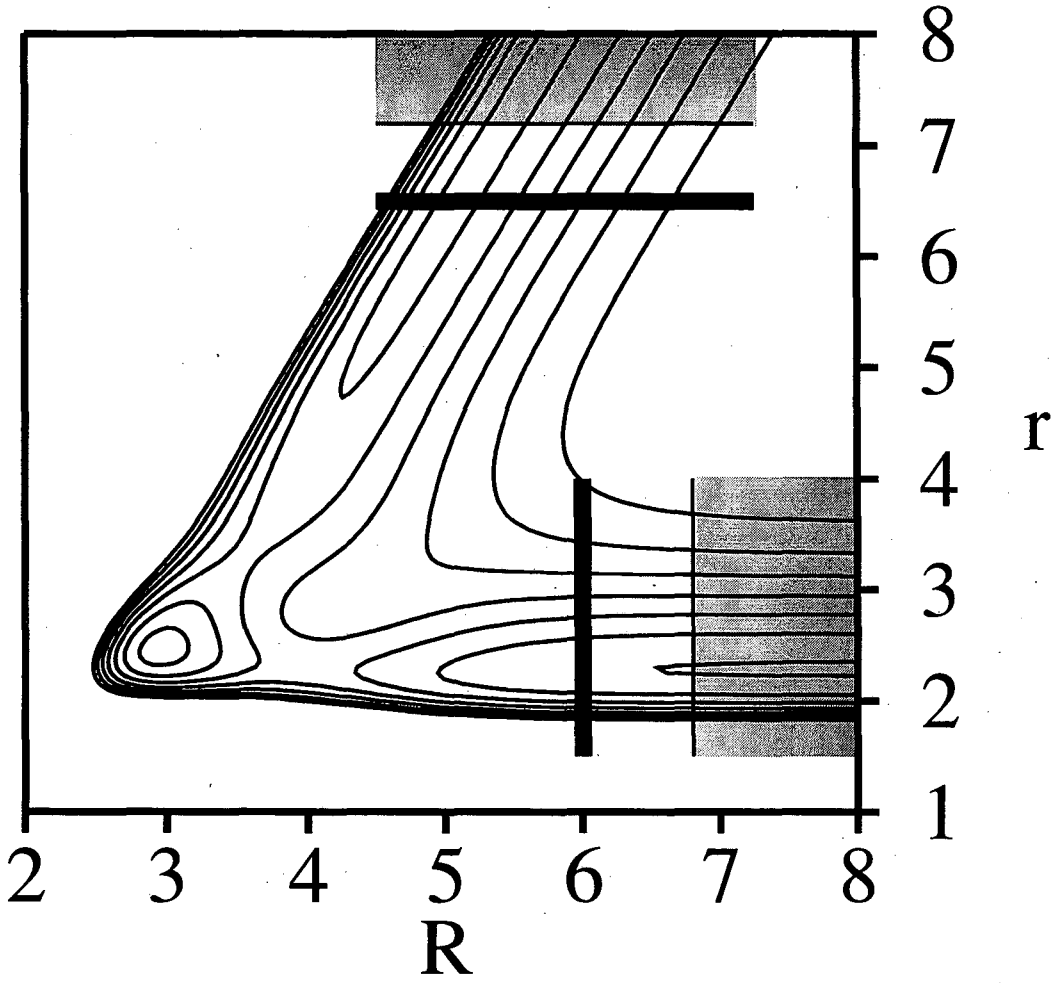

Figure 3.2: Contour plot of the HO_2 DMBE IV potential energy surface[29] for a colinear ($\gamma = 0$) geometry. The reactant and product dividing surfaces are shown by thick lines. The shaded areas are absorbing potentials $\hat{\epsilon}(R, r)$ which start at the thin lines and increase to the edge of the DVR grid. R and r are shown in atomic units.

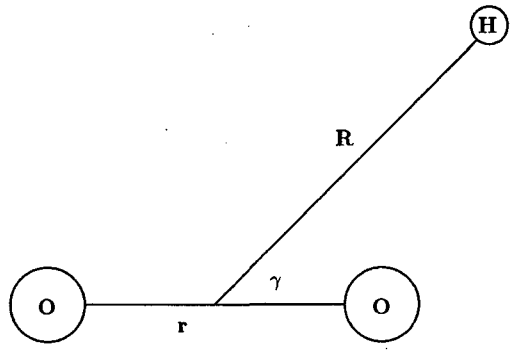

Figure 3.3: The Jacobi coordinates for the molecular system.

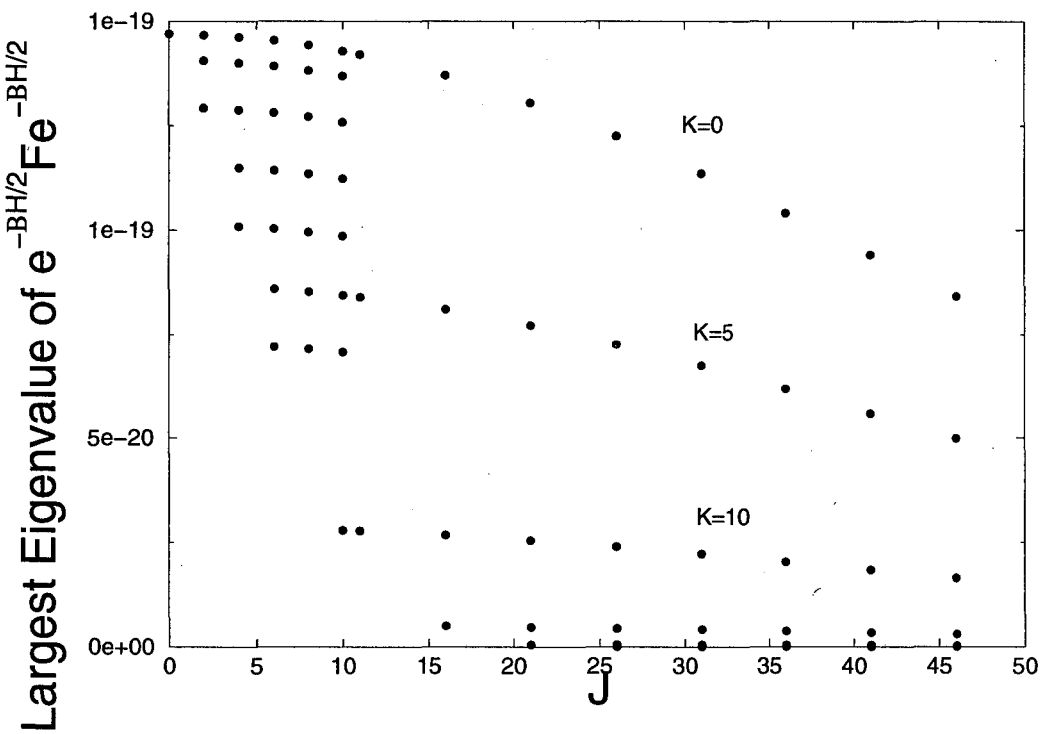

Figure 3.4: The largest eigenvalue of the thermal flux operator as a function of the rotational quantum numbers J and K.

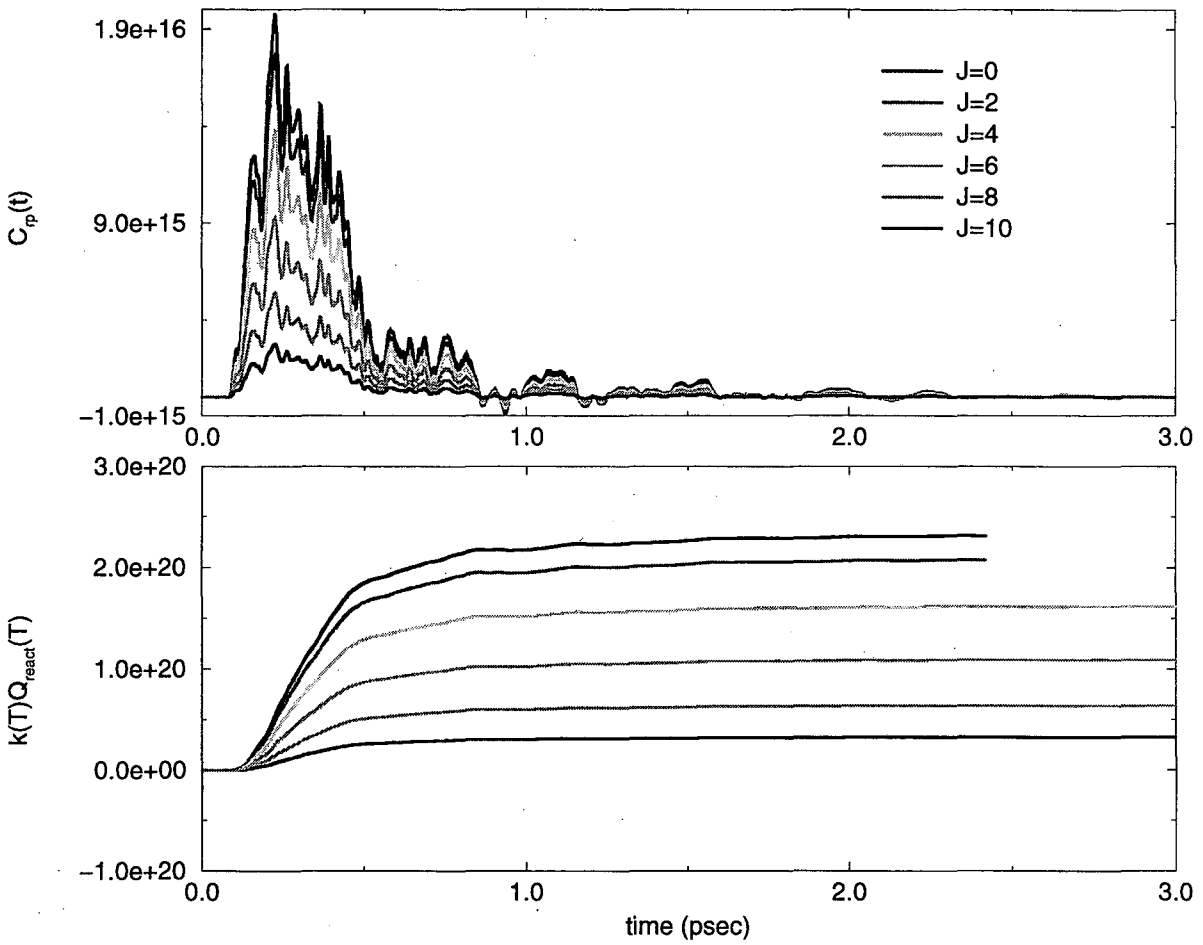

Figure 3.5: The J selected thermal flux cross correlation functions (T = 600K) and their integrals. The dynamics in the reaction region is nearly over after about 2 psec and the integral contribution converges to a constant value.

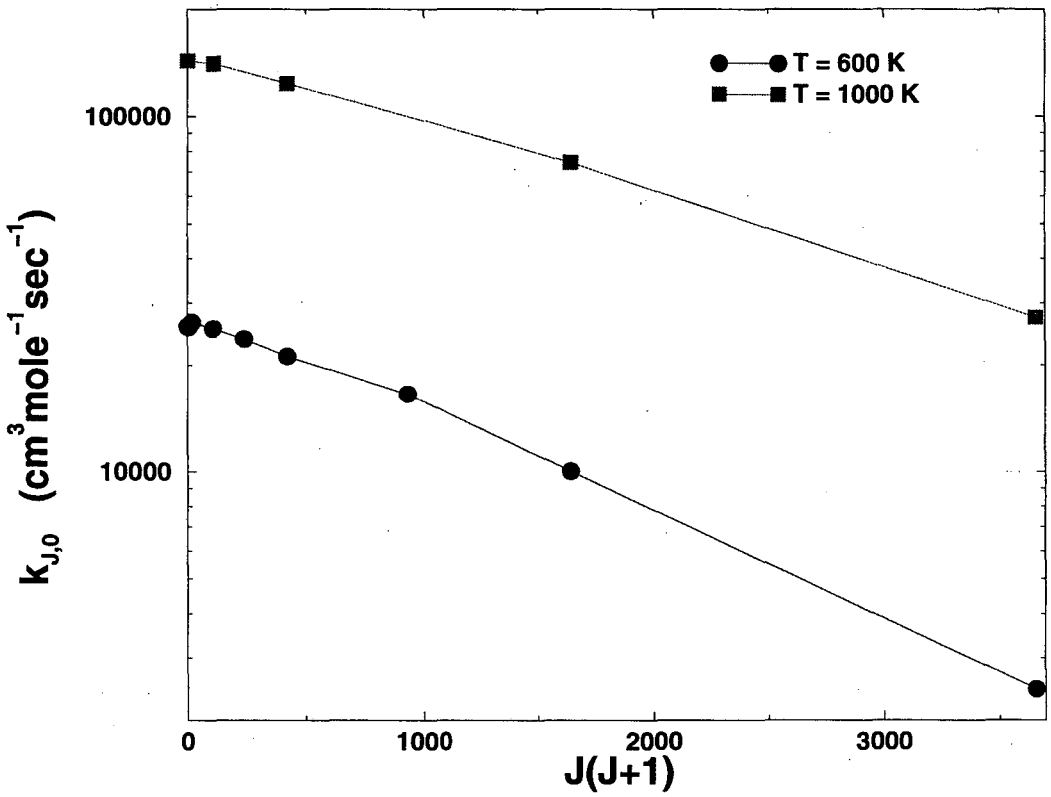

Figure 3.6: Here is shown the individual $k_J(T)$, from Equation(3.2), computed within the Helicity Conserving Approximation. Rates at two temperatures are shown 600K and 1000K. The line connecting the points shows the interpolation scheme used in order to evaluate Equation(3.1).

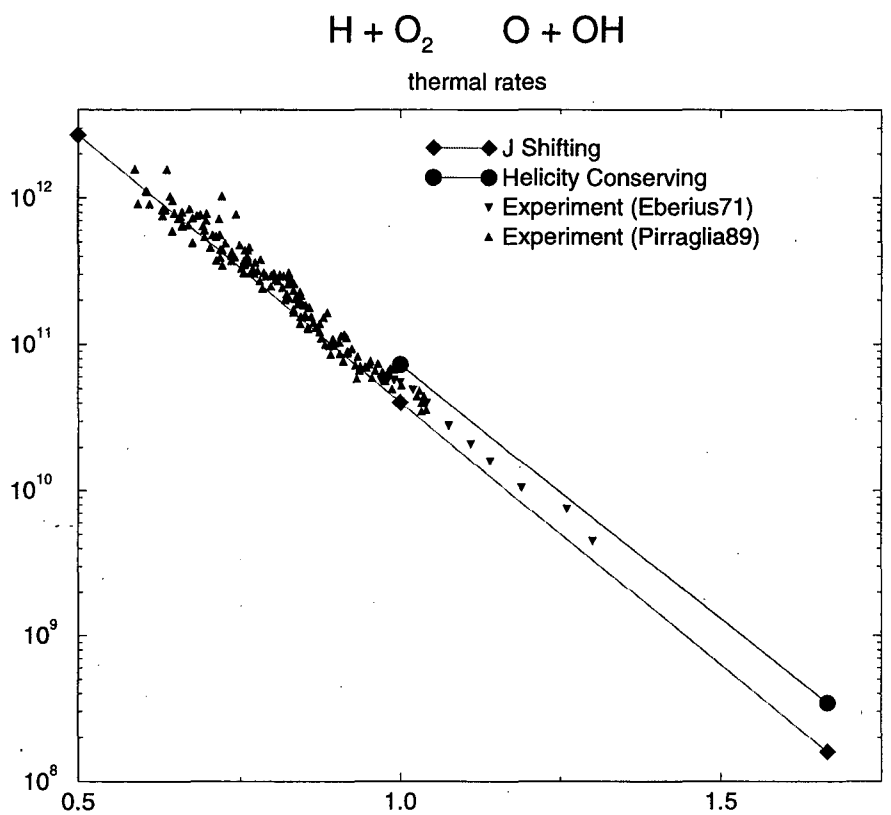

Figure 3.7: Total Thermal Rates for $H + O_2 \rightarrow O + OH$ calculated here compared to experimentally determined values.

$$\hat{T}_R = \hat{U}^\dagger_{FFT}\, diag\left(\frac{-\hbar^2(j - N_R/2)}{2\mu\Delta R^2}\right)\hat{U}_{FFT} \tag{3.10a}$$

$$\hat{T}_r = \hat{U}^\dagger_{FFT}\, diag\left(\frac{-\hbar^2(j - N_r/2)}{2m\Delta r^2}\right)\hat{U}_{FFT} \tag{3.10b}$$

$$\hat{T}_\gamma = \hat{U}^\dagger_{Leg}\, diag\left(-\hbar^2 J(J+1)\left(\frac{1}{2\mu R^2} + \frac{1}{2mr^2}\right)\right)\hat{U}_{Leg}, \tag{3.10c}$$

where *diag* is a matrix with only diagonal entries (indexed by j), N_R and N_r are 64 and 128 respectively, and $\hat{U}_{Leg}$ is the Legendre transformation which includes the first 32 odd associated Legendre polynomials. (Only odd Legendre polynomials in $cos(\gamma)$ are included because the wavefunctions must be odd under interchange of the two identical oxygen atoms[29].)

A time step $\Delta t = 10$ au was used for the thermal propagation and 20 au for the real time propagation. For all calculations the number of thermal flux eigenvectors included is determined by the temperature alone. At T=600 K 20 eigenvectors were propagated and at T = 1000 K 40 eigenvectors were propagated. The real-time propagation of the eigenvectors is the most time consuming part of the calculation. These calculations were carried out on a Cray T3D parallel computer and required approximately 1 hour per eigenvector in the 64 processor queue.

The dividing surface for reactants $(O + OH)$ is defined by $r = 6.5a_0$ and that for products $(H + O_2)$ by $R = 6a_0$. The same dividing surfaces were used for all calculations. Several dividing surfaces other than the ones mentioned were tried. It was found that the effort involved in the calculation, *i.e.*the length of real time propagation, varied significantly with the choice of dividing surface. The appropriate compromise is to place the surfaces far enough out that there is minimal recrossing flux, but not so far out as to delay the approach to the reaction region. This is evidenced in Figure(3.5) as the positive lobe of the correlation function occurs quickly (in $\sim$ 100 nsec) and also in that there minimal negative contribution to the rate from flux recrossing the dividing surface.

As in several other studies of HO_2 we use the DMBE IV potential energy surface of Pastrana *et al.*[30] for our calculations.

Absorbing potentials, $\hat{\epsilon}(q)$, were placed just beyond each of these dividing surfaces to prevent reflection of reactive flux from the edge of the DVR basis. The reactant and product absorbing potentials start at $r = 7.2a_0$ and $R = 6.8a_0$, respectively. Both are quartic potentials which rise from zero to a maximum of 0.3 to 0.5 eV. Figure3.2 shows a schematic of the dividing surfaces and absorbing potentials.

Figure 3.5 shows typical results for the flux correlation function, here for T = 600 K and for several values of total J. The $\sim$ 1 psec time scale for the decay of the correlation function, *i.e.*, the lifetime of the collision complex, is seen not to vary much with J. The integral contribution to the total rate is seen to drop rapidly with J.

3.3 Approximate Treatments for $J > 0$

3.3.1 The Helicity Conserving Approximation

Figure 3.3 shows the Jacobi coordinates that we use — **r** is the O-O coordinate and **R** is that of H and the center of mass of O-O — in terms of which the Hamiltonian has the standard form

$$\hat{H} = \hat{T}_R + \hat{T}_r + \frac{\hat{\boldsymbol{\ell}}^2}{2\mu R^2} + \frac{\hat{\boldsymbol{\jmath}}^2}{2mr^2} + V(R, r, \gamma), \tag{3.11}$$

where

$$\hat{T}_R = -\frac{\hbar^2}{2\mu}\frac{\partial^2}{\partial R^2}, \qquad \hat{T}_r = -\frac{\hbar^2}{2m}\frac{\partial^2}{\partial r^2},$$

$\hat{\boldsymbol{\ell}}$ and $\hat{\boldsymbol{\jmath}}$ are the angular momentum operators for the R and r angular motion respectively, and V is the potential energy surface. The usual helicity (or j_z) conserving approximation[31] is to choose **R** as the body-fixed quantization axis and to assume that the projection of total angular momentum along it is conserved, *i.e.*, to neglect off-diagonal matrix elements in the quantum number K, the projection quantum number for this body-fixed axis.

This would be a poor choice for the present reaction, however, because the kinematics of the light H atom makes this component of the total angular momentum

poorly conserved during the dynamical motion. Choosing the best body-fixed axis for purposes of making a helicity conserving approximation (*i.e.* neglect of $\Delta K \neq 0$ matrix elements) is the same choice microwave spectroscopists make in deciding on the best "almost symmetric top" axis for molecular rotation[32]; *e.g.*, if the body-fixed axis were indeed a symmetric top axis, then K would be conserved without approximation. From these considerations it is clear that because of the light mass of the H atom a much better (*i.e.* nearly symmetric top) choice for the body-fixed axis is the O-O axis, *i.e.*, the vector $\mathbf{r}$. This idea of using the heavy atom axis in a "heavy + light-heavy" mass combination has often been used in the past[33], the analogy of the electron in H_2^+ often being invoked. We also note that it was used by Thompson and Miller in their treatment[21] of the $O + HCl \rightarrow OH + Cl$ reaction.

With $\mathbf{r}$ thus chosen as the body-fixed axis, one follows Van Vleck's prescription and uses total angular momentum conservation to eliminate the angular momentum for this axis ($\hat{\mathfrak{j}}$).

$$\hat{\mathfrak{j}} = \hat{\mathbf{J}} - \hat{\boldsymbol{\ell}}, \tag{3.12}$$

so that the Hamiltonian becomes

$$\hat{H} = \hat{T}_R + \hat{T}_r + \frac{\hat{\boldsymbol{\ell}}^2}{2\mu R^2} + \frac{|\hat{\mathbf{J}} - \hat{\boldsymbol{\ell}}|^2}{2mr^2} + V. \tag{3.13}$$

The HCA is obtained by taking the part of the Hamiltonian diagonal in K, which gives

$$\hat{H}_{JK} = \hat{H}_{J=0} + E_{JK}(R, r, \gamma) \tag{3.14a}$$

where

$$\hat{H}_{J=0} = \hat{T}_R + \hat{T}_r + \hat{T}_\gamma + V(R, r, \gamma) \tag{3.14b}$$

with

$$\hat{T}_\gamma = -\hbar^2\left(\frac{\partial^2}{\partial\gamma^2} + \cot\gamma\frac{\partial}{\partial\gamma}\right)\left(\frac{1}{2\mu R^2} + \frac{1}{2mr^2}\right) \tag{3.14c}$$

and

$$E_{JK}(R,r,\gamma) = \frac{J(J+1)-2K^2}{2mr^2} + \frac{K^2}{\sin^2\gamma}(\frac{1}{2\mu R^2} + \frac{1}{2mr^2}). \tag{3.14d}$$

The effective potential energy surface for $J > 0$ alluded to in Section 3.2 is thus

$$V_{JK}(R,r,\gamma) = V(R,r,\gamma) + E_{JK}(R,r,\gamma), \tag{3.15}$$

the actual potential plus a centrifugal potential that is the rotational energy of the molecular complex as a function of the coordinates (R,r,γ) that determine its shape. We note that E_{JK} can also be written in standard symmetric top form,

$$E_{JK}(R,r,\gamma) = B(R,r,\gamma)(J(J+1)-K^2) + C(R,r,\gamma)K^2 \tag{3.16a}$$

where the rotational 'constants' are (with $\hbar = 1$)

$$B(R,r,\gamma) = \frac{1}{2mr^2} \tag{3.16b}$$

$$C(R,r,\gamma) = (\frac{1}{2\mu R^2} + \frac{\cos^2\gamma}{2mr^2})/\sin^2\gamma \tag{3.16c}$$

In practice, rather than suming over all (J,K), we need only complete the calculation of $k_{JK}(T)$ for several (J,K) pairs and note the dependence on the rate on these parameters. If the dependence of the rate is smooth we can extrapolate the sum in Equation(3.1). For the present reaction this dependence can be seen in Figure(3.4). The largest eigenvalue of the thermal flux operator, which is a bound to the contribution to the total rate, is seen to be a smoothly and rapidly decreasing function of J.

3.3.2 The J-shifting Approximation

The J-shifting approximation (JSA) results by assuming that the rotational constants in Equation(3.16) are truly constants,

$$B(R,r,\gamma) \to B^{\ddagger} \equiv B(R^{\ddagger},r^{\ddagger},\gamma^{\ddagger}) \tag{3.17a}$$

$$C(R, r, \gamma) \rightarrow C^{\ddagger} \equiv C(R^{\ddagger}, r^{\ddagger}, \gamma^{\ddagger}) \tag{3.17b}$$

corresponding to some reference geometry $(R^{\ddagger}, r^{\ddagger}, \gamma^{\ddagger})$. Since the Hamiltonian for $J > 0$ then only differs from that of $J = 0$ by a constant, it is easy to see that the equations in Section 3.2 lead to

$$k_{JK}(T) = k_{J=0}(T)e^{-\beta E^{\ddagger}_{JK}} \tag{3.18a}$$

where

$$E^{\ddagger}_{JK} = B^{\ddagger}(J(J+1) - K^2) + C^{\ddagger}K^2. \tag{3.18b}$$

The sums over J and K in Equation(3.1) and (3.2) then give

$$k(T) = k_{J=0}(T)Q^{\ddagger}_{rot} \tag{3.18c}$$

where $Q^{\ddagger}_{rot}$ is the rotational partition function,

$$Q^{\ddagger}_{rot} = \sum_{J=0}^{\infty}(2J+1)\sum_{K=-J}^{J} e^{-\beta E^{\ddagger}_{JK}} \tag{3.18d}$$

which is usually accurately approximated by its classical limit

$$Q^{\ddagger}_{rot} = \frac{kT}{B^{\ddagger}}\sqrt{\frac{\pi kT}{C^{\ddagger}}} \tag{3.18e}$$

if $B^{\ddagger}$ and $C^{\ddagger} \leq kT$.

At the level of the JS approximation it is not neccessary to assume that the rigid molecular system has a symmetric top geometry. If it is that of an asymmetric rotor, *i.e.*, all three rotational constants $A^{\ddagger}$, $B^{\ddagger}$, and $C^{\ddagger}$ are different, then the classical partition function of Equation(3.18e) becomes

$$Q^{\ddagger}_{rot} = \sqrt{\frac{\pi(kT)^3}{A^{\ddagger}B^{\ddagger}C^{\ddagger}}} \tag{3.18f}$$

which can be thought of as the same as the symmetric top expression Equation(3.18e) with the replacement $B^{\ddagger} \rightarrow \sqrt{A^{\ddagger}B^{\ddagger}}$.

A comparison of the JS approximation and the HC approximation discussed above is seen in Figure (3.7). Comparison is also made with experimentally determined values of the thermal reaction rate. The JS approximation results and those of the HC approximation bracket the experimental values on either side.

3.3.3 Principal Axis Helicty Conserving Approximation

For the present molecular system the O-O axis **r** is a very nearly symmetric top axis because of the lightness of the H atom, but in other cases it may be that neither **R** nor **r** is a good choice. Thus some years ago McCurdy and Miller[34] suggested using one of the instantaneous principal axes of the molecular system as the body-fixed axis for purposes of making a HC approximation. This was motivated by the way microwave spectroscopists[32] make the "best symmetric top" approximation for molecular rotation and also by the desire to have a body-fixed axis that changes continuously from reactants to products during a chemical reaction.

McCurdy and Miller used the classical form of the Hamiltonian, obtained by taking the classical limit of the quantum Hamiltonian operator given by Diehl[35] *et al.*,

$$\begin{aligned} &H(R, p_R, r, p_r, \gamma, p_\gamma, K, q_K) = \\ &\frac{1}{2\mu}(p_R - \Delta p_R)^2 + \frac{1}{2m}(p_r - \Delta p_r)^2 \\ &+(\frac{1}{2\mu R^2} + \frac{1}{2mr^2})(p_\gamma - \Delta p_\gamma)^2 \\ &+V(R, r, \gamma) + \frac{J_1^2}{2I_1} + \frac{J_2^2}{2I_2} + \frac{J_2^3}{2I_3} \end{aligned} \tag{3.19}$$

where q_K is the angle variable conjugate to the projection "quantum number" (actually action variable) K, and the other coordinates and moments are as before. J_i, $i = 1, 2, 3$ are the components of the angular momentum along the three instantaneous principal axes, and I_i are the corresponding principal moments of inertia, ordered so that $I_1 < I_2 < I_3 = I_1 + I_2$ (for this planar molecular system); specifically

$$I_2 - I_1 = \sqrt{(\mu R^2)^2 + (mr^2)^2 + 2\mu R^2 mr^2 \cos(2\gamma)} \tag{3.20a}$$

$$I_2 + I_1 = \mu R^2 + mr^2 \tag{3.20b}$$

The vibrational angular momentum terms $\Delta p_R, \Delta p_r, \Delta p_\gamma$ in Equation(3.19) are given by

$$\Delta p_R = -J_3 \frac{2I_1 I_2}{(I_2 - I_1)^2} \frac{\cos\gamma}{R} \tag{3.21a}$$

$$\Delta p_r = J_3 \frac{2I_1 I_2}{(I_2 - I_1)^2} \frac{\cos\gamma}{r} \tag{3.21b}$$

$$\Delta p_\gamma = -J_3 \frac{2I_1 I_2}{(I_2 - I_1)^2} \frac{(\mu R^2 - mr^2)\sin\gamma}{I_1 + I_2} \tag{3.21c}$$

and if principal axis 1 (the one with the smallest moment of inertia) is chosen as the body-fixed quantization axis, then

$$J_1 = K \tag{3.22a}$$

$$J_2 = \sqrt{J^2 - K^2}\cos q_K \tag{3.22b}$$

$$J_3 = \sqrt{J^2 - K^2}\sin q_K. \tag{3.22c}$$

The classical version of the HC approximation, which corresponds to the quantum prescription of taking the matrix elements of $\hat{H}$ diagonal in K, is obtained by *averaging* the classical Hamiltonian over the angle variable q_k. In doing this, McCurdy and Miller neglected the contribution from the vibrational angular momentum terms, but it is not necessary to do so. The averaging process is straight-forward,

$$\langle \cdots \rangle \equiv \frac{1}{2\pi}\int_0^{2\pi} dq_K \cdots ,$$

so that

$$\begin{aligned} \langle K \rangle &= K \\ \langle \sin q_K \rangle &= \langle \cos q_K \rangle = 0 \\ \langle \sin^2 q_K \rangle &= \langle \cos^2 q_K \rangle = \frac{1}{2} \end{aligned}$$

and it is not hard to carry this out to obtain an HC Hamiltonian of the same form as Equation(3.14a),

$$\begin{aligned} H_{JK}(R, p_R, r, p_r \quad &, \gamma, p_\gamma) = \\ &H_{J=0} + B(R, r, \gamma)(J^2 - K^2) + C(R, r, \gamma)K^2 \end{aligned} \tag{3.23}$$

where $H_{J=0}$ is the same as Equation(3.14b) and here,

$$C(R, r, \gamma) = \frac{1}{2I_1} \tag{3.24a}$$

$$B(R, r, \gamma) = \frac{1}{4}(\frac{1}{I_2} + \frac{I_2 + I_1}{(I_2 - I_1)^2}). \tag{3.24b}$$

In the limit $\mu R^2 \ll mr^2$ it is not hard to show that the rotational constants in Equation(3.24) revert to those in Equation(3.16).

3.3.4 Some Further Thoughts on $J > 0$ Approximations

The helicity conserving approximations discussed above try to identify a body-fixed axis which is an almost symmetric top axis for the molecular geometries relevant to the dynamics, so that K (the helicity) is conserved during the dynamics, speaking classically, or a good quantum number, speaking quantum mechanically.

From a very different perspective Bowman[36] has suggested using an *adiabatic rotation* (AR) approximation, which would be justified dynamically if the rotational motion (*i.e.*, q_K, classically) were fast compared to the internal (R, r, γ) motion. In this case one proceeds as in the Born-Oppenheimer approximation, *i.e.*, freezes the (R, r, γ) degrees of freedom and solves for the rotational energy levels of the (in general) asymmetric rotor, $E_{J,\tau}(R, r, \gamma)$, as a function of the internal geometry. The Hamiltonian for the internal motion is then

$$\hat{H}_{J\tau} = \hat{H}_{J=0} + E_{J\tau}(R, r, \gamma), \tag{3.25}$$

i.e., of the same form as that for the HCA, Equation(3.14) or Equation(3.23). In fact, if the asymmetric rotor energy levels are approximated as an almost symmetric top–which is often a very good approximation– then

$$E_{J\tau}(R, r, \gamma) \rightarrow B(R, r, \gamma)(J(J+1) - K^2) + C(R, r, \gamma)K^2, \tag{3.26}$$

which is then identical to the principal axis HC approximation if the vibrational angular momentum terms are neglected (as McCurdy and Miller originally did).

To complete this discussion the range of possible approximations for $J > 0$ it is useful to consider the opposite limit for the rotational motion, namely that it is much *slower* than the internal (R, r, γ) motion. This is the rotational sudden approximation (SA) which has a long history in molecular collision theory[37]. In the present context this would mean freezing the rotational variables (J, K, q_K) in the Hamiltonian Equation(3.19), computing the rate constant as a parametric function of these variables, and then averaging that result over the variables for the rotational degrees of freedom. The net rate constant would thus be given by

$$k(T) = \int_0^\infty dJ\ 2J \int_{-J}^{J} dK \int_0^{2\pi} \frac{dq_K}{2\pi}\ k(T; J, K, q_k), \tag{3.27a}$$

where $k(T; J, K, q_k)$ is the rate constant computed from the Hamiltonian that depends parametrically on (J, K, q_K),

$$H(J, K, q_K) = H_{J=0} + \frac{J_1^2}{2I_1} + \frac{J_2^2}{2I_2} + \frac{J_3^2}{2I_3} \tag{3.27b}$$

$$= H_{J=0} + \frac{K^2}{2I_1} + (J^2 - K^2)(\frac{\cos^2 q_K}{2I_2} + \frac{\sin^2 q_K}{2I_3}) \tag{3.27c}$$

where we have for simplicity dropped the vibrational angular momentum terms (they could be retained if desired). This approximation is somewhat more costly to implement than the PA/HCA because the result of the calculation now depends on the three parameters (J, K, q_K) rather than just two, (J, K). In the symmetric top limit, $I_2 \simeq I_3$, however, one sees that the q_K dependence in Equation(3.27c) disappears and one is again back to the same expression as the PA/HCA. Thus if the internal dynamics is confined to molecular geometries that are well approximated as a symmetric top, one obtains the same effective Hamiltonian whether rotation is treated as fast or slow. Finally, it is easy to show that Equation(3.27a) for the sudden approximation can be written as

$$k(T) = \frac{1}{2\pi} \int d_3\mathbf{J}\ k(T; \mathbf{J}), \tag{3.28a}$$

with

$$H_{\mathbf{J}} = H_{J=0} + \frac{1}{2}\mathbf{J} \cdot \mathbf{I}(R, r, \gamma)^{-1} \cdot \mathbf{J} \tag{3.28b}$$

which makes it clear that this approximation is completely independent of how the body-fixed axis is chosen; *e.g.*, it is not even necessary in Equation(3.28b) that the inertia tensor be diagonal. By evaluating the integral over **J** in spherical coordinates (J, θ, ϕ),

$$\int d_3\, \mathbf{J} = \int_0^\infty dJ\; J^2 \int_0^\pi d\theta \sin\theta \int_0^{2\pi} d\phi \tag{3.29}$$

one can show that Equation(3.28a) is equivalent to Equation(3.27a).

3.4 Results and Discussion

The HCA described in Section 3.3.1 was used for the $J > 0$ calculations reported here. This should be an excellent approximation for this reaction because the O-O axis is such a good "almost symmetric top" axis; *e.g.*, in Table 3.4 one sees how close are the two smallest rotational constants, $A^\ddagger$ and $B^\ddagger$, at both the geometry of the HO_2 minimum and the $O\cdots OH$ transition state. One also sees how close are the exact rotational constants of the $O\cdots OH$ transition state and those implied by the HCA (Equation(3.16)) at this geometry.

Within the HCA, however, the calculation of $k_{JK}(T)$ for each (J, K) is equivalent in effort to the $k_{J=0}(T)$ calculation, which is itself already a very expensive calculation due to the the small grid spacing that is necessary because of the deep potential well and also the long propagation times resulting from the long-lived complex. It is therefore very important to minimize the number of (J, K) values for which calculations are actually performed. To this end the (J, K) dependence of $k_{JK}(T)$ was fit to the following functional form

$$\ln[k_{JK}(T)/k_{00}(T)] = -\beta\{aJ + b|K| + B[J(J+1) - K^2] + CK^2\} \tag{3.30}$$

which is sufficiently accurate for the range of J and K values that contribute. Adding terms of higher order in J and K did not affect to result for the total rate constant. Between 15 and 19 $k_{JK}(T)$ were calculated to perform this fit at each temperature. The values of a,b,B,C determined from the fit and used for the interpolation are given

in Table 3.4. The sum over J and K to obtain the total rate thus gives the same form as the JSA,

$$k(T) = k_{J=0}(T) Q_{rot}(T), \tag{3.31a}$$

where here

$$Q_{rot}(T) = \sum_{J=0}^{\infty} \sum_{K=-J}^{J} e^{-\beta\{aJ+b|K|+B[J(J+1)-K^2]+CK^2\}}. \tag{3.31b}$$

Table 3.4 lists the rate constants given by the HCA at T = 600 K and 1000 K, and also those given by the JSA with two possible choices of the reference geometry, that of the HO_2 minimum and that of the $O \cdots OH$ transition state. (Here we note an error in the use of the JSA in our previous paper[3]; the rotational constants used there for the HO_2 minimum — $A^\ddagger = 0.572 cm^{-1}$, $B^\ddagger = 0.589 cm^{-1}$, $C^\ddagger = 18.94 cm^{-1}$ — are in error; the correct values are those in Table 3.4.)

Comparing the (presumably) accurate HCA results with those of the JSA in Table 3.4, one sees that the JSA is not bad — the rate constant agrees with that of the HCA to 10-20% for this temperature range — *provided* one uses the $O \cdots OH$ transition state as the reference geometry for the rotational motion. For a 'direct' reaction it is commonly believed — with some examples to support it[18,38] — that the transition state geometry is the best reference geometry for the JSA, but since the collision complex ($HO_2^\ddagger$) spends most of its time in the region about the HO_2 minimum, it was not obvious that this latter geometry might not be a better choice in this case. The minimum *does* seem to be the best choice for the JSA in describing resonance energies[39] of the HCO complex, a very similar system. For the rate constant, however, we see that in this case, too, the transition state geometry is the best choice for the JSA.

This latter observation, *i.e.*, that the transition state geometry provides the best choice of reference geometry for the JSA in both 'complex-forming' as well as 'direct' reactions, is thus an encouraging one, for the JSA is by far the simplest way of dealing with $J > 0$ if the choice of reference geometry is unambiguous. The full

Table 3.1: Rotational Constants and Partition Functions at Fixed Geometries.

Geometry	$A^{\ddagger}$ $/cm^{-1}$	$B^{\ddagger}$ $/cm^{-1}$	$C^{\ddagger}$ $/cm^{-1}$	$Q^{\ddagger}_{rot}(600K)$	$Q^{\ddagger}_{rot}(1000K)$
HO_2 minimum[a]	1.051	1.115	20.51	3069	6603
$O\cdots OH$ TS[a]	0.286	0.287	44.52	7897	16971
HCA TS[b]	0.290	0.290	45.00	9647	19350

[a]Exact rotational constants of the three atom system at the indicated geometry.

[b]Rotational constants of the $O\cdots OH$ geometry implied by the HCA Equation(3.16)

Table 3.2: Parameters Describing the Dependence of $k_{JK}(T)$ on J and K in Equation(3.30)

Temperature $/K$	a $/cm^{-1}$	b $/cm^{-1}$	B $/cm^{-1}$	C $/cm^{-1}$
600	-3.14	77.7	0.318	1.65
1000	-2.37	62.7	0.336	18.3

dynamical calculation is then required only for $J = 0$, an enormous simplification. It is important, however, to have the possibility of carrying out more accurate treatments of $J > 0$, as discussed in Section 3.3, to calibrate its reliability, as in the present application.

Finally, we note from Table 3.4 that the rate constants given by the HCA(and the JSA with the $O\cdots OH$ reference geometry) with this potential surface are in quite good agreement with the experimental values. To pursue matters further it would be useful to utilize the more recent and presumably more accurate potential energy surface developed by Kendrick and Pack[40] and also to deal explicitly with the electronically non-adiabatic dynamics arising from the spin-orbit coupling in this system.

Table 3.3: Rate Constants in $cm^3 molecule^{-1} sec^{-1}$ for $H + O_2 \rightarrow O + OH$

Method	$k(600\ K) \times 10^{16}$	$k(1000\ K) \times 10^{14}$
JSA (HO_2 minimum)	1.32	3.52
JSA ($O \cdots OH$ TS)	3.39	9.03
HCA	4.12	10.3
Experiment*	3.72	9.1

*The rate constant at 600 K was extrapolated from a measurement of $k^{-1}(520K)$ by Howard and Smith[41] using the experimentally determined equilibrium constant[42]. The rate constant at 1000 K was measured by Eberius *et al.*[43]

Chapter 4

Semiclassical Approaches

4.1 Semiclassical Initial Value Representation

As mentioned at the outset of this work, molecules span a range of sizes, that is masses, which sit firmly with quantum mechanics on the small end and fall into the realm of classical mechanics for larger molecules. The chasm between these worlds is the realm of semiclassical theories. In the theory presented here we are essentially trying to develop a form of classical molecular dynamics, motivated by quantum mechanics, which expresses quantum effects when they are important and ignores them when they are not.

The semiclassical (SC) initial value representation[102,103] (IVR) is undergoing a re-birth of interest as a practical way for including quantum interference and tunneling effects into classical molecular dynamics simulations[46–67]. The primary difference in the recent IVR approaches from the original version is that they are now implemented in the cartesian coordinate (or coherent state) representation rather than in action-angle variables, and this is more general, better behaved numerically, and also typically more accurate. The number of successful applications in recent years gives one confidence that the SC-IVR does indeed provide a good description of quantum effects for a wide range of molecular phenomena (including electronically non-adiabatic processes[64,67]).

Applications of the SC-IVR approach to date, however, have mostly dealt with

molecular systems of a relatively few degrees of freedom because of the oscillatory nature of the integrand in the phase space average over initial conditions of classical trajectories. Applications that have included larger numbers of degrees of freedom have almost always done so with harmonic bath modes which have a particularly smooth semiclassical structure. Finding methods to cope with the fundamentally oscillatory nature of the integrand is very active area of research[114–119]. In this spirit, after the general theory is presented, we will present two methods of taming the SC-IVR integrand.

A *linearization approximation*[63,64] to the SC-IVR has been considered which simplifies this oscillatory structure of the IVR integrand. This linearized SC-IVR (LSC-IVR) has been seen to be capable of describing quantum effects correctly in the *short time* regime (time $\leq \hbar\beta$) of thermal reactive flux correlations functions, but not the longer time behavior.

We also present the Forward-Backward version (FB-IVR) of the SC-IVR. The goal of the FB-IVR is to again simplify the oscillatory structure of the IVR integrand, but through a distinctly different approximation.

4.2 Theoretical Development

As a starting point for our examination of semiclassical dynamics consider the time evolved overlap,

$$\langle\phi|e^{-it\hat{H}\hbar}|\psi\rangle, \tag{4.1}$$

which provides a transition amplitude which between two states. Expanding this expression in the position coordinate variables $\mathbf{q}_0$ and $\mathbf{q}_t$ gives,

$$\int d\mathbf{q}_t \int d\mathbf{q}_0 \langle\phi|\mathbf{q}_t\rangle\langle\mathbf{q}_t|e^{-it\hat{H}\hbar}|\mathbf{q}_0\rangle\langle\mathbf{q}_0|\psi\rangle, \tag{4.2}$$

The Feynmann path integral interpretation of the quantity $\langle\mathbf{q}_t|e^{-it\hat{H}\hbar}|\mathbf{q}_0\rangle$ is that of summing all possible paths between $\mathbf{q}_0$ and $\mathbf{q}_t$ weighted by the complex phase, $e^{iS/\hbar}$, where S is an action quantity associated with the path.

Van Vleck developed a useful approximation[121] to this quantity by completing a stationary phase integration of the path integral. The resulting expression consists of a sum over paths which are restricted to follow classical paths. The Van Vleck version of Equation(4.1) is given by,

$$\sum_{S'=0} \int d\mathbf{q}_t \int d\mathbf{q}_0 \langle \phi | \mathbf{q}_t \rangle e^{iS_{cl}(\mathbf{q}_0, \mathbf{q}_t, t)} \left((i2\pi\hbar)^F \left| \frac{\partial \mathbf{q}_t}{\partial \mathbf{q}_0} \right| \right)^{-1/2} \langle \mathbf{q}_0 | \psi \rangle, \tag{4.3}$$

where the sum extends over all classical paths between $\mathbf{q}_0$ and $\mathbf{q}_t$, roots of S'. The dimensionality of coordinate space is F. The classical action is given by,

$$S_{cl}(\mathbf{q}_0, \mathbf{q}_t, t) = \int_{t_0}^{t} dt' \left[\mathbf{p}_{t'} \cdot \dot{\mathbf{q}}_{t'} - H(\mathbf{p}_{t'}, \mathbf{q}_{t'}) \right] \tag{4.4}$$

The Van Vleck expression is problematic as it requires the determination of the classical paths between two specified points in fixed time. In general there are multiple paths since we are free to choose a variety of initial momenta. This root search is a two point boundary value problem and for chaotic systems the determination of all such paths proves quite difficult. To make things worse the denominator in Equation(4.3) can be singular.

The initial value representation (IVR) is born out of doing away with the root search by recognizing the factor, $|\partial \mathbf{q}_t / \partial \mathbf{q}_0|$ as the Jacobian for a transformation between $\mathbf{q}_t, \mathbf{q}_0$ and $\mathbf{p}_0, \mathbf{q}_0$. After making this change of coordinates Equation(4.1) becomes,

$$\int d\mathbf{q}_t \int d\mathbf{q}_0 \langle \phi | \mathbf{q}_t \rangle e^{iS_{cl}(\mathbf{q}_0, \mathbf{q}_t, t) - i\pi\nu/2} \left(\left| \frac{\partial \mathbf{q}_t}{\partial \mathbf{q}_0} \right| / (i2\pi\hbar)^F \right)^{1/2} \langle \mathbf{q}_0 | \psi \rangle. \tag{4.5}$$

This IVR, sometimes called the primitive IVR, is a great improvement over Equation(4.3). Since it is an initial value problem there is no longer a root search problem. What's more the denominator is no longer singular. The new factor ν, the Maslov index, is an integer which ensures that the integrand is continuous and is easily computed.

The above derivation of Equation(4.5) was done in the position coordinate representation. A similar derivation holds true in the momentum representation. And

interesting balance of the two is the derivation of an IVR in the coherent state representation, which interpolates between the previous two. The applications here use the Herman-Kluk[51,52], or coherent state version of the SC-IVR, which expresses a quantum time evolution operator as,

$$e^{-i\hat{H}t/\hbar} = (2\pi\hbar)^{-F} \int d\mathbf{p}_0 \int d\mathbf{q}_0 C_t(\mathbf{p}_0, \mathbf{q}_0) e^{iS_t(\mathbf{p}_0,\mathbf{q}_0)/\hbar} |\mathbf{p}_t, \mathbf{q}_t\rangle\langle \mathbf{p}_0, \mathbf{q}_0|, \tag{4.6}$$

where $(\mathbf{p}_0, \mathbf{q}_0)$ are initial conditions of the coordinates and momenta for classical trajectories. $\mathbf{p}_t(\mathbf{p}_0, \mathbf{q}_0; t)$, $\mathbf{q}_t(\mathbf{p}_0, \mathbf{q}_0; t)$ are the momenta and coordinates at time t that evolve from these initial conditions, and S_t is the classical action integral along the trajectory. The pre-factor C_t involves the monodromy matrix elements,

$$C_t = \left| \frac{1}{2} \left(\frac{\partial \mathbf{q}_t}{\partial \mathbf{q}_0} + \frac{\partial \mathbf{p}_t}{\partial \mathbf{p}_0} - i\gamma\hbar \frac{\partial \mathbf{q}_t}{\partial \mathbf{p}_0} + \frac{i}{\gamma\hbar} \frac{\partial \mathbf{p}_t}{\partial \mathbf{q}_0} \right) \right|^{1/2}. \tag{4.7}$$

The bra and ket states in Equation(4.6) are coherent states, the coordinate space wave functions of which are of the form

$$\langle \mathbf{x}|\mathbf{p}_0, \mathbf{q}_0\rangle = (\frac{\gamma}{\pi})^{F/4} e^{-\frac{\gamma}{2}|\mathbf{x}-\mathbf{q}_0|^2 + i\mathbf{p}_0\cdot(\mathbf{x}-\mathbf{q}_0)/\hbar}, \tag{4.8}$$

and F is again the number of degrees of freedom of the molecular system. Coherent states have the property of being analogous to classical phase space points centered at $\mathbf{p}_0, \mathbf{q}_0$ but with a distribution about this center which is appropriate for quantum mechanics.

For many systems it seem that the integrand of the Herman-Kluk propagator is less oscillatory than that of the Equation(4.5). The smoother integrand makes Equation(4.6) the best starting place for many semiclassical calculations.

Chapter 5

Semiclassical Molecular Energy Transfer

5.1 Introduction

In this chapter we will apply the methods just discussed to the determination of energy transfer between molecules in a collision. We do not consider reactive collisions though there has been some work[108,115] in this direction.

Calculations are carried out for the well known colinear $He + H_2(v_i) \rightarrow He + H_2(v_f)$ problem studied by Secrest and Johnson[68]. This example provides a good testbed for semiclassical approximations to quantum mechanics since we know that quantum interference plays an important role in the inelastic scattering product state distribution.

5.2 LSC-IVR for the S-matrix

Here we will present a test of the SC-IVR approach, and especially the LSC-IVR, on a problem which has well-understood quantum interference features. This is the well-studied[102,103,68–70] model of inelastic scattering for which Secrest and Johnson[68] carried out coupled channel quantum calculations many years ago, the colinear $He + H_2(v_i) \rightarrow He + H_2(v_f)$ problem . This was the first example to which "classical

S-matrix" theory was applied[102] in 1970, showing prominent interference features in the distribution of final vibrational states due to interference between two classical trajectories that typically contribute to each transition probability. Here we wish first to verify that the full SC-IVR treatment is able to describe this well (as it does), and primarily to see how much error is introduced by its linearized approximation.

As noted before[66], the LA results in classical propagation and overlap of Wigner distribution functions, a result given by a variety of other formulations and approximations[71–73]. In the present application it is very close, though not completely identical, to a model Lee and Scully[74] put forth some years ago and tested on this very same example. Comparison to the Lee and Scully version of the approximation will thus also be presented.

We consider a multichannel scattering problem characterized by a Hamiltonian of the form,

$$H(P, R, \mathbf{p}, \mathbf{r}) = \frac{P^2}{2\mu} + h(\mathbf{p}, \mathbf{r}) + V(R, \mathbf{r}) \tag{5.1}$$

where (P, R) are the momentum and coordinate for the relative translation of the two collision partners, and $(\mathbf{p}, \mathbf{r})$ are the momenta and coordinates of the internal degrees of freedom. A rigorous quantum expression for the S-matrix in terms of the time evolution operator (propagator) is[75]

$$S_{2,1}(E) = \frac{-\hbar\sqrt{k_1 k_2}}{\mu} e^{-i(k_1 R_1 + k_2 R_2)} \int_0^\infty dt e^{itE/\hbar} \langle R_2 \phi_2 | e^{-it\hat{H}/\hbar} | R_1 \phi_1 \rangle \tag{5.2}$$

where E is the total energy, $\hbar k_n, n = 1, 2$ are the initial and final translational momenta,

$$k_n = \sqrt{2\mu(E - \mathcal{E}_n)/\hbar^2} \tag{5.3}$$

and $\mathcal{E}_n$ and $\phi_n(\mathbf{r}), n = 1, 2$ are the eigenvalues and eigenfunctions of the internal Hamiltonian $h(\mathbf{p}, \mathbf{r})$; the limit $R_1, R_2 \to \infty$ is implied in Equation(5.2), but these values only have to be so large that the interaction potential $V(R, \mathbf{r})$ is negligible.

The coordinate space (or Van Vleck) IVR approximates the propagator as a phase space average over initial conditions for classical trajectories,

$$e^{-it\hat{H}/\hbar} = \int d\mathbf{p}_0 \int d\mathbf{q}_0 \sqrt{\left|\frac{\partial \mathbf{q}_t(\mathbf{p}_0, \mathbf{q}_0)}{\partial \mathbf{p}_0}\right| / (2\pi i\hbar)^F}\; e^{iS_t(\mathbf{p}_0,\mathbf{q}_0)/\hbar} |\mathbf{q}_t\rangle\langle\mathbf{q}_0| \tag{5.4a}$$

where $(\mathbf{p}, \mathbf{q})$ denote all F degrees of freedom of the complete system (*i.e.*, $\mathbf{q} = (R, \mathbf{r})$, *etc.*), $\mathbf{q}_t(\mathbf{p}_0, \mathbf{q}_0)$ is the coordinate at time t that evolves along the classical trajectory with initial conditions $(\mathbf{p}_0, \mathbf{q}_0)$, and S_t is the action along it,

$$S_t(\mathbf{p}_0, \mathbf{q}_0) = \int_0^t dt' (\mathbf{p} \cdot \dot{\mathbf{q}} - H). \tag{5.4b}$$

Using the SC-IVR for the propagator, Equation(5.4a), in Equation(5.2) for the S-matrix thus gives

$$S_{2,1}(E) = \frac{-\hbar}{\mu}\sqrt{k_1 k_2} e^{-i(k_1 R_1 + k_2 R_2)} \int_0^\infty dt \int d\mathbf{p}_0 \int d\mathbf{r}_0 \int dP_0 \int dR_0 \tag{5.5}$$
$$\sqrt{\left|\frac{\partial(\mathbf{r}_t, R_t)}{\partial(\mathbf{p}_0, P_0)}\right| / (2\pi i\hbar)^F}\; e^{iEt/\hbar} e^{iS_t(\mathbf{p}_0,\mathbf{r}_0,P_0,R_0)/\hbar} \delta(R_t - R_2)\phi_2(\mathbf{r}_t)^* \phi_1(\mathbf{r}_0)\delta(R_0 - R_1),$$

and the two delta functions in the integrand allow the integrals over R_0 and t to be evaluated, so that the final SC-IVR result for the S-matrix is

$$S_{2,1}(E) = -e^{-i(k_1 R_1 + k_2 R_2)} \int d\mathbf{p}_0 \int d\mathbf{r}_0 \int dP_0 \sqrt{\left|\frac{\partial(\mathbf{r}_t, R_t)}{\partial(\mathbf{p}_0, P_0)}\right| / (2\pi i\hbar)^F} \tag{5.6}$$
$$e^{i[Et + S_t(\mathbf{p}_0,\mathbf{r}_0,P_0,R_0)]/\hbar} \phi_2(\mathbf{r}_t)^* \phi_1(\mathbf{r}_0) \hbar \sqrt{k_1 k_2}/P_t$$

(The factor of $1/P_t$ arises from $\int dt \delta(R_t - R_2) = 1/\dot{R}_t$.) The trajectories in Equation(5.6) begin with initial conditions $\mathbf{r}_0, \mathbf{p}_0, P_0$,and $R_0 = R_1$ (an arbitrary fixed, large value), and terminate when $R_t = R_2$ (an arbitrary fixed, large value), this latter relation being what determines the value of t in the integrand of Equation(5.6).

Equation(5.6) is what we have used to compute the SC-IVR transition probabilities,

$$P_{2,1}(E) = |S_{2,1}(E)|^2 \tag{5.7}$$

discussed below in Section 5.3. We also carried out calculations using the Herman-Kluk coherent state version[51,52] of the IVR and obtained essentially identical results.

The *linearized approximation* (LSC-IVR) is obtained by explicitly squaring the SC-IVR S-matrix of Equation(5.6) to obtain the transition probability via Equation(5.7), giving an expression of the form,

$$P_{2,1}(E) = \int d\mathbf{r}_0 \int d\mathbf{p}_0 \int dP_0 \int d\mathbf{r}_0' \int d\mathbf{p}_0' \int dP_0' \{\ldots\} \tag{5.8}$$
$$e^{i[Et+S_t(\mathbf{p}_0,\mathbf{q}_0,P_0,R_0)-Et'-S_{t'}(\mathbf{p}_0',\mathbf{q}_0',P_0',R_0')]/\hbar}$$

The LSC-IVR corresponds to expanding the difference of the action integrals in the integrand of Equation(5.8) to linear order in $(\mathbf{r}_0-\mathbf{r}_0')$, *etc.*, with the corresponding approximation for the pre-exponential Jacobian factors . The details of this calculation have been given before[66], and one obtains the following

$$P_{2,1}^{LSC-IVR}(E) = (2\pi\hbar)^{-(F-1)} \int d\mathbf{p}_0 \int d\mathbf{r}_0 \frac{\hbar^2 k_1 k_2}{|P_0 P_t|} \rho_2(\mathbf{r}_t, \mathbf{p}_t)^* \rho_1(\mathbf{r}_0, \mathbf{p}_0), \tag{5.9a}$$

where again $R_0 = R_1$ and $R_t = R_2$ determines t, and the initial translational momentum is given by,

$$P_0 = -\sqrt{2\mu(E - h(\mathbf{p}_0, \mathbf{r}_0))}. \tag{5.9b}$$

$\{\rho_n\}, n = 1, 2$ in Equation(5.9a) are the Wigner distribution functions for the initial and final internal states

$$\rho_n(\mathbf{r}, \mathbf{p}) = \int d\mathbf{r}' e^{-i\mathbf{p}\cdot\mathbf{r}'/\hbar} \phi_n(\mathbf{r} + \frac{1}{2}\mathbf{r}')\phi_n(\mathbf{r} - \frac{1}{2}\mathbf{r}')^* \tag{5.9c}$$

Finally, as noted before[66], the LSC-IVR expression in Equation(5.9a) is very similar to one put forth many years ago by Lee and Scully[74] (LS) and tested on the

same system we treat presently, the only difference being that LS take the initial momentum to be the quantum value,

$$P_0 = -\hbar k_1 = -\sqrt{2\mu(E - \mathcal{E}_1)} \tag{5.10}$$

rather than the value in Equation(5.9b) that is determined by total energy conservation and the initial conditions of the internal degrees of freedom. The transition probability given by the LSC-IVR procedure is microscopically reversible, *i.e.*,

$$P_{2,1}^{LSC-IVR} = P_{1,2}^{LSC-IVR} \tag{5.11}$$

while that given in the LS prescription is not. Nevertheless, it will be seen that even though the LSC-IVR result, Equation(5.9b), is on sounder theoretical ground, the LS version, *i.e.*, with Equation(5.10) replacing Equation(5.9b), gives better numerical results for the present example (though neither the LS or LSC-IVR versions are nearly as accurate as the full SC-IVR results based on Equation(5.6)).

5.3 Inelastic Scattering in $He + H_2(v_i) \rightarrow He + H_2(v_f)$

The Secrest-Johnson[68] model of colinear $A + BC(v_i) \rightarrow A + BC(v_f)$ vibrationally inelastic scattering corresponds to the Hamiltonian of Equation(5.1) for one internal degree of freedom, a harmonic oscillator, for which

$$H(P, R, p, r) = \frac{P^2}{2\mu} + h(p, r) + V(R, r) \tag{5.12a}$$

and with the following internal Hamlitonian and interaction potential,

$$h(p, r) = \frac{p^2}{2m} + \frac{1}{2}m\omega^2 r^2 \tag{5.12b}$$

$$V(R, r) = e^{\alpha(r-R)}. \tag{5.12c}$$

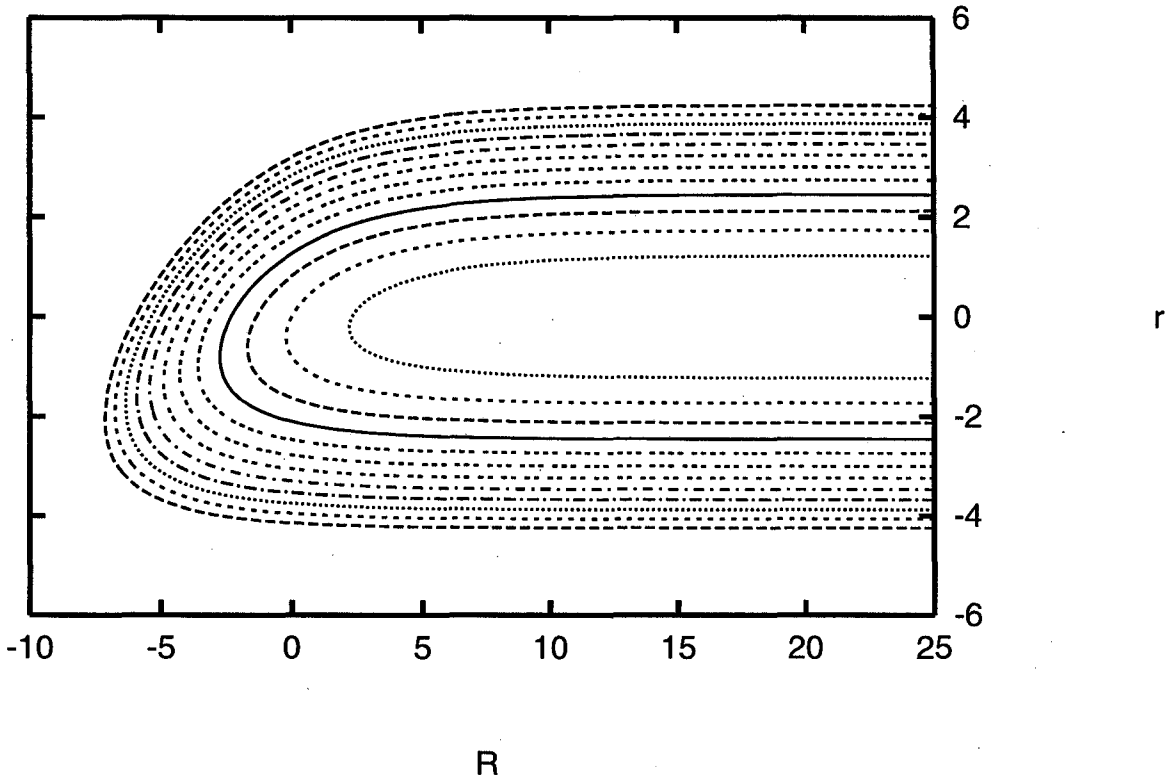

Figure 5.1: The Secrest-Johnson surface for inelastic scattering.

In the reduced units used by Secrest and Johnson, $m = 1, \omega = 1, \alpha = 0.3$, and $\mu = 2/3$ for the $He + H_2$ system. The Secrest-Johnson potential energy surface is shown in Figure (5.1).

Figures 5.2 and 5.3 show the comparison of the exact quantum results for the vibrational transition probabilities $P_{v_f,v_i}(E)$ and the SC-IVR results given by Equation(5.6), for two different total energies. One sees that the SC-IVR results agree extremely well with the correct QM values in all cases. The interference structure in P_{v_f,v_i} versus v_f —*i.e.*, the product state distribution— is well understood from the earlier classical S-matrix treatment[102] of this system as arising from the interference of two classical trajectories that emerge from the stationary phase approximation to the IVR integral over initial conditions.

For the present application the SCI-IVR expression [Equation(5.6)] involves only a three dimensional integration, which was evaluated by a quasi-random space filling

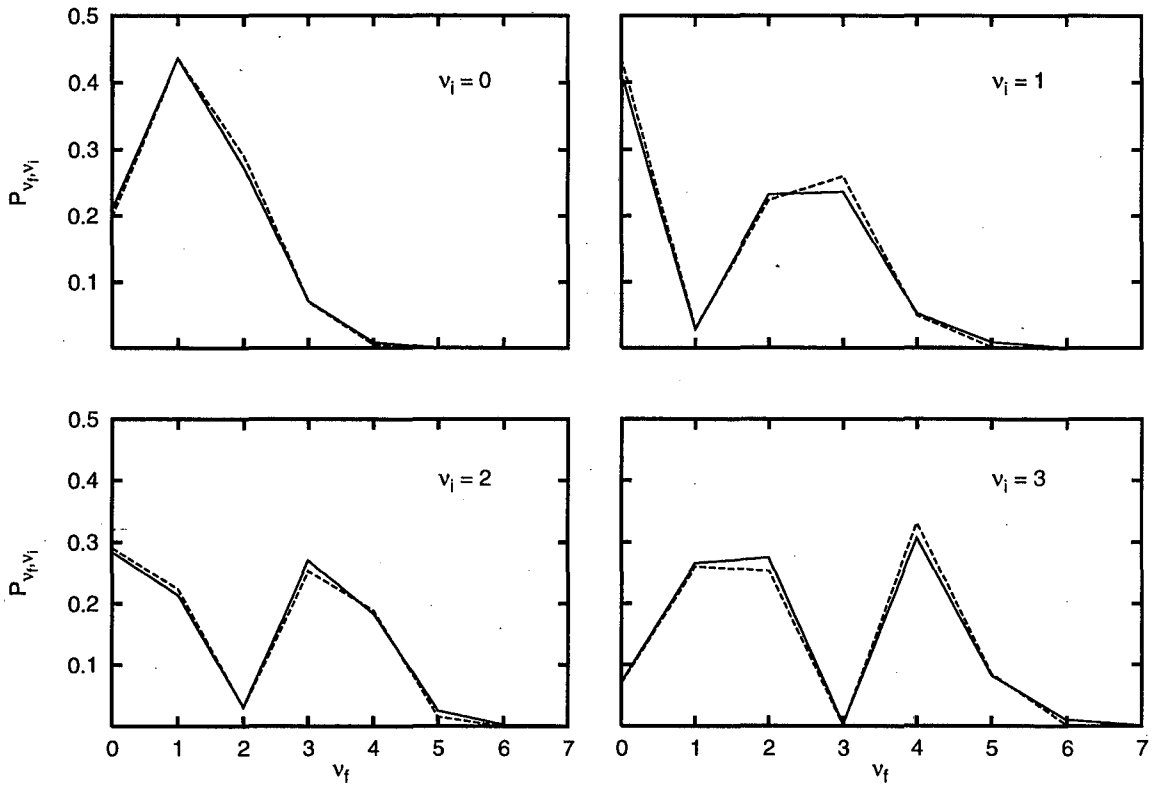

Figure 5.2: Vibrational transition probabilities as a function of final vibrational quantum number v_f, for several initial vibrational states v_i, and total energy $E = 8$. The solid lines connect the exact quantum values, and the dashed lines are those given by the SC-IVR, Equation(5.6).

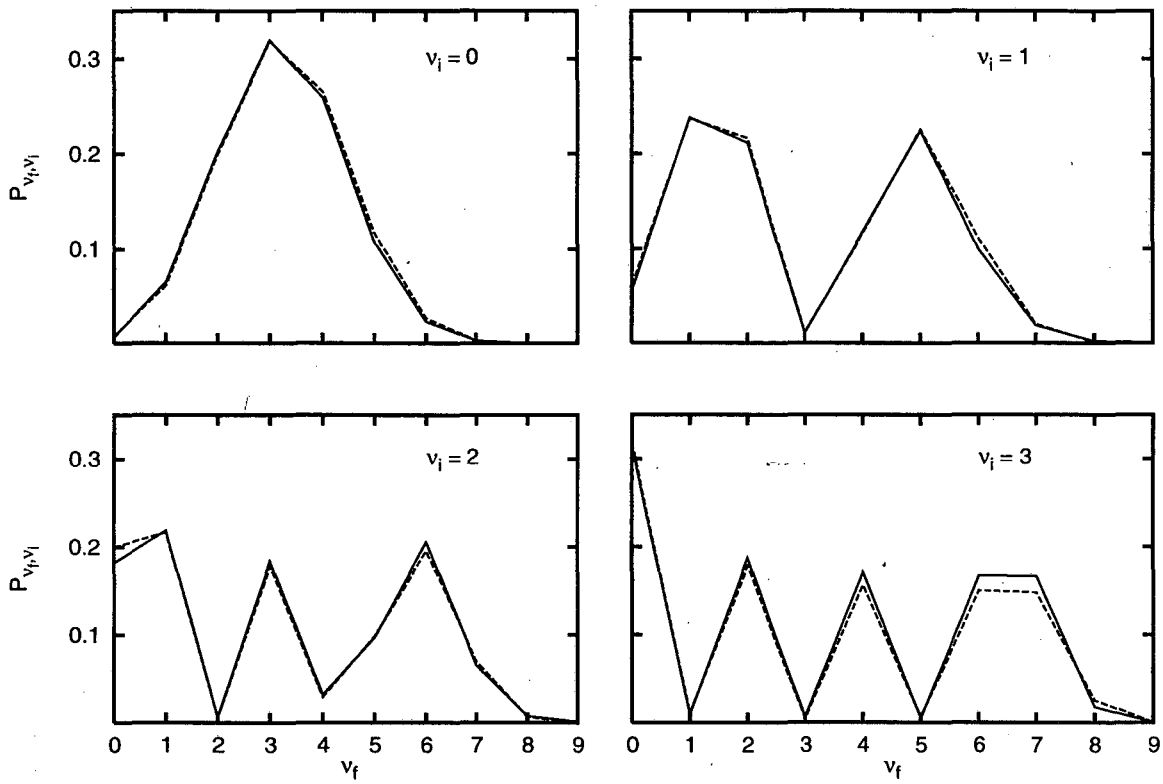

Figure 5.3: Vibrational transition probabilities as a function of final vibrational quantum number v_f, for several initial vibrational states v_i, and total energy $E = 12$. The solid lines connect the exact quantum values, and the dashed lines are those given by the SC-IVR, Equation(5.6).

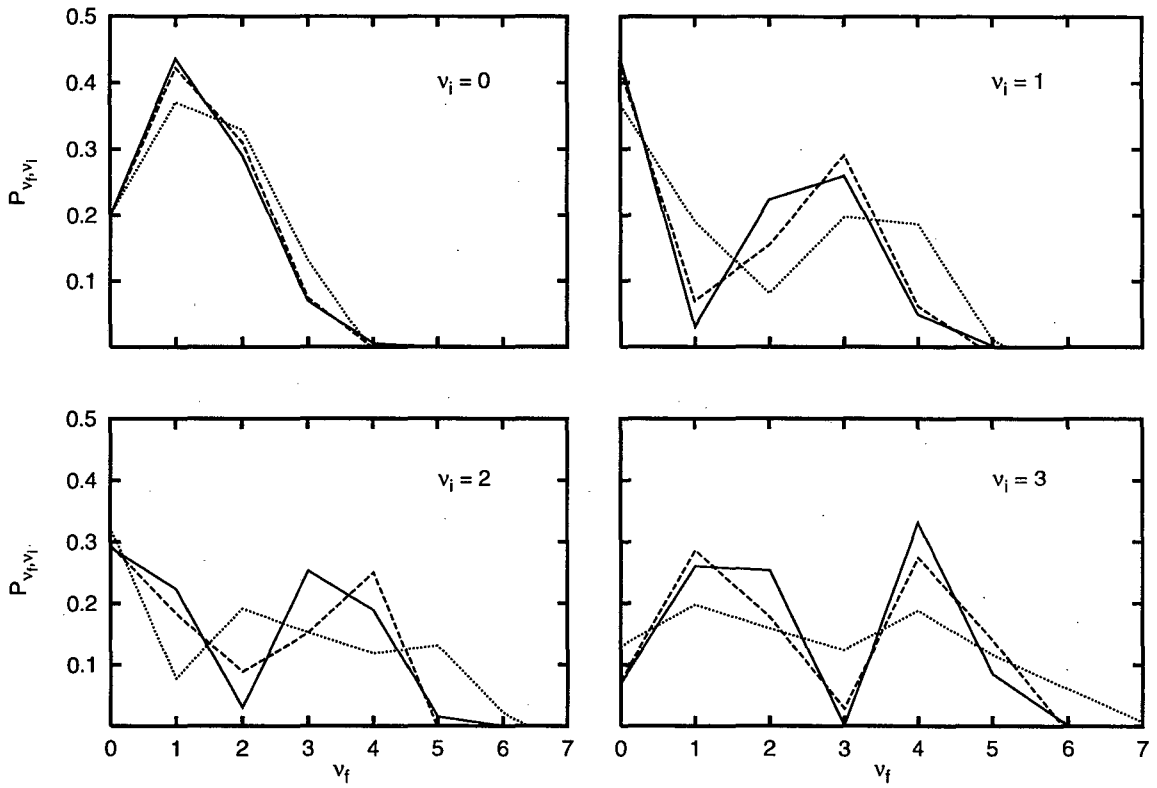

Figure 5.4: Vibrational transition probabilities as a function of final vibrational quantum number v_f, for several initial vibrational states v_i, and total energy $E = 8$. The dotted lines connect the values given by the linearized approximation (LSC-IVR) to the SC-IVR, Equation(5.9a), and the dashed lines those of the Lee-Scully (LS) version of the LSC-IVR, Equation(5.10).

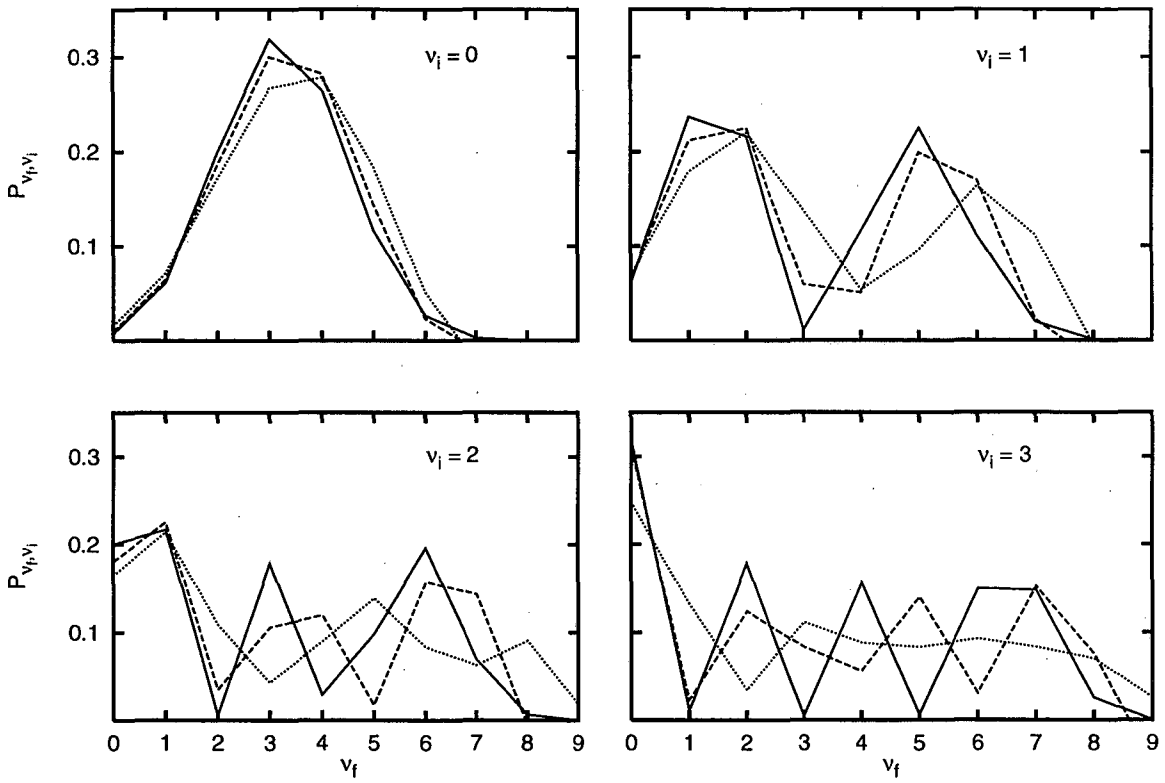

Figure 5.5: Vibrational transition probabilities as a function of final vibrational quantum number v_f, for several initial vibrational states v_i, and total energy $E = 12$. The dotted lines connect the values given by the linearized approximation (LSC-IVR) to the SC-IVR, Equation(5.9a), and the dashed lines those of the Lee-Scully (LS) version of the LSC-IVR, Equation(5.10).

method[76]. Since the integration points are independent of the initial and final states (and the energy), one can evaluate the entire matrix of transition probabilities for all energies with one batch of classical trajectories. It required $\simeq 10^4 - 10^5$ classical trajectories to obtain convergence in the transition probabilities. For higher dimensional problems one will typically wish to use Monte Carlo methods to perform the integration over initial conditions, with filtering methods to smooth the oscillatory integrand, and importance sampling that may depend on the initial and final states.

Figures 5.4 and 5.5 show the same quantum results but compared here to the *linearized approximation* (LSC-IVR) of Equation(5.9a). One sees that the LSC-IVR results are in reasonable agreement on the average, but they do not describe the quantum interference structure very accurately. The original Lee-Scully version of this approximation, using Equation(5.10) rather than Equation(5.9b), is seen to do somewhat better than the more theoretically justifiable version, a result hard to rationalize.

For state-to-state transitions such as these, the LSC-IVR actually represents only a minor savings in effort compared to the full SC-IVR approach; *i.e.* Equation(5.6) shows that the full IVR calculation requires a $2F-1$ dimensional integral and the LSC-IVR of Equation(5.9a) reduces this only to a $2F-2$ dimensional integral. The LSC-IVR has the simplifying feature, however, of not requiring elements of the monodromy matrix (the pre-exponential Jacobian factor in Equation(5.4a)), though it requires the additional effort of calculating the Wigner transforms of the initial and final states rather than needing only their wavefunctions. At the full state-to-state description there is thus little point in not carrying out the full SC-IVR calculation, especially given the fact that it is more accurate. This conclusion applies only for state-to-state processes, however; the LSC-IVR leads to a much simpler approach than the full SC-IVR treatment for the calculation of time correlation functions.

5.4 LSC-IVR Results

The purpose of this calculation has been two-fold, first to verify that the current version of the semiclassical initial value representation is able to provide a good de-

scription of quantum effects in this well-studied benchmark for inelastic scattering, and second to test the degree of error introduced by using the linearized approximation (LSC-IVR) to the SC-IVR. The first goal is clearly met, *i.e.*, the SC-IVR describes the quantum structure in the vibrational transition probabilities quite accurately. Secondly, the LSC-IVR describes the average value of the transition probability fairly well, but the interference features much less so.

This behavior of the LSC-IVR is consistent with our earlier experiences with it. For the collinear $H + H_2 \rightarrow H_2 + H$ reaction, for example, it described[66] the *average* energy dependence of the reaction probability quite well, but not the resonance structure, which arises semiclassically from the interference of different reactive trajectories. Similarly, in using the LSC-IVR for reactive flux correlation functions[63,66] it was seen to describe quantum effects well in the short time regime, but the longer time dynamics was essentially that given by classical mechanics. A quantitative description of the quantum interference/coherence structure thus requires the full SC-IVR approach. This gives one further incentive to develop methods that will make such calculations more efficient. In this regard, we note that the recently suggested[77,90] "forward-backward" algorithm shows considerable promise, at least for time correlation functions. On the other hand, for applications where interference/coherence features are unimportant (*i.e.*, expected to be averaged out), the LSC-IVR provides a very useful and much simpler approach.

Finally, although the expressions in Section 5.2 were written explicitly for non-reactive scattering, it should be clear from general semiclassical theory[75] that Equation(5.6) applies to reactive scattering essentially as written; the only modification is that in the final wavefunction, $exp(-ik_2R_2)\phi_2(\mathbf{r}_2)$, the coordinates $(R_2, \mathbf{r}_2)$ are the Jacobi coordinates for the final (product) arrangement of atoms rather than those of the initial (reactant) arrangement.

5.5 Molecular Energy Transfer via FB-IVR

Molecular energy transfer (*i.e.*, inelastic scattering) is a critical component of many processes in chemical kinetics. In the Lindemann model of unimolecular de-

composition (or recombination), for example[79,80], it is the energy transfer step,

$$A_i + B \rightarrow A_f + B, \tag{5.13}$$

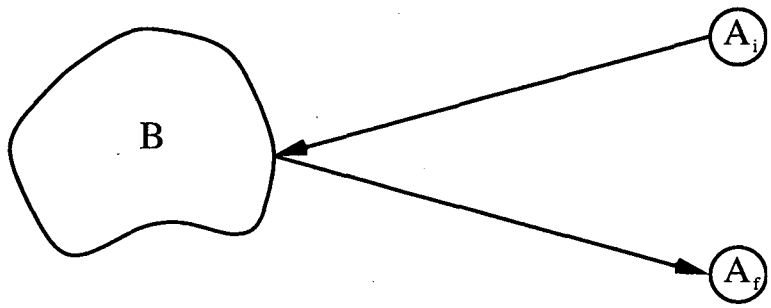

that excites molecule A (via collision with bath molecules B) to a metastable state that undergoes decomposition (or de-excites a metastable state to a stable one after recombination).

In most applications one is not interested in the detailed state-to-state inelastic scattering probability (or cross section), but rather the average probability (or cross section) for molecule A to transfer a given amount of internal energy per collision, $P(\Delta E_A)$, $\Delta E_A = E_f^A - E_i^A$ where E_i^A (E_f^A) is the initial (final) internal energy of molecule A. Very often[79] one simply assumes a functional form for this probability, *e.g.*,

$$P(\Delta E_A) \propto e^{-|\Delta E_A|/\Delta} \tag{5.14a}$$

or

$$P(\Delta E_A) \propto e^{-\Delta E_A^2/\Delta^2} \tag{5.14b}$$

and though experiments[81] have shown that these assumptions are often qualitatively reasonable, there can be significant departures. (We also note an interesting debate[82,83] about the existence and significance of a long tail to the energy transfer probability, so-called 'super collisions'). There has also been important work recently in more rigorous theoretical calculation of energy transfer probabilities, using both classical trajectory and quantum mechanical approaches[84–87].

Here we show how the recently introduced forward-backward (FB) version of the semiclassical (SC) initial value representation (IVR)[77,88–90] can be used to calculate the energy transfer probability (or cross section). Specifically, the energy transfer probability (or cross section) is expressed as the Fourier transform of a time correlation function,

$$P_i(\Delta E_A) = \int_{-\infty}^{\infty} dt\ e^{i\Delta E_A t/\hbar} C_i(t) \tag{5.15}$$

where $C_i(t)$ is given by a single phase space average over the initial conditions of the $A + B$ collision system.

One should note earlier work by Micha[91–98] *et al.* and by Heller[99–101] *et al.* using time correlation functions to describe inelastic scattering. The present work is closest in spirit to that of Heller, Reimers, and Drolshagen[99] on neutron scattering, though the quantities involved are clearly different, and these authors used the frozen Gaussian approximation to semiclassical theory.

The semiclassical (SC) initial value representation (IVR) that we presently adapt to molecular energy transfer was first developed and applied in action angle variables[102,103], and has recently been the focus of renewed interest as a method for including quantum mechanical effects in molecular dynamics[77,88,89,46–59,104–114,67]. Recently the SC-IVR has been extended and applied in novel ways with the aim of making large scale quantum molecular dynamics simulations more practical. Among the new IVR approaches are the Herman-Kluk[51,52] (HK), linearized semiclassical[110,113] (LSC), and forward-backward[77,88–90](FB) IVRs. Given the recently developed variations on the IVR approach, it is useful to determine which and to what extent these approximations preserve important quantum mechanical effects such as tunneling and coherence. Comparison with state specific quantum mechanical results provides a particularly rigorous test of these semiclassical methods.

In previous sections of this work we showed that state-to-state energy transfer in the Secrest-Johnson (SJ) model of inelastic scattering is accurately described by the full SC-IVR , while the LSC-IVR gives only a qualitative description of the quantum interference. Now we examine the FB-IVR treatment of molecular energy transfer.

5.5.1 Probability Distribution of Molecular Energy Transfer

We consider the inelastic bimolecular collision of molecule A with (bath) molecule B,

$$A_i + B_j \rightarrow A_{i'} + B_{j'}, \tag{5.16}$$

which is governed by a total Hamiltonian of the form,

$$\hat{H} = \frac{\hat{\mathbf{P}}^2}{2\mu} + \hat{h}_A + \hat{h}_B + \hat{V} \tag{5.17}$$

where $\hat{h}_A$ ($\hat{h}_B$) is the Hamiltonian for molecule $A(B)$, and $\hat{\mathbf{P}}$ is the 3d momentum operator for relative translation of A and B.

The classical momenta and coordinates for molecule A, molecule B and their relative translation are $(\mathbf{p}_A, \mathbf{q}_A)$, $(\mathbf{p}_B, \mathbf{q}_B)$, $(\mathbf{P}, \mathbf{R})$, respectively, and $\mathbf{p} \equiv (\mathbf{p}_A, \mathbf{p}_B, \mathbf{P})$, $\mathbf{q} \equiv (\mathbf{q}_A, \mathbf{q}_B, \mathbf{R})$ denote all the F coordinates and momenta. The interaction potential $\hat{V}(\mathbf{q})$ involves all the coordinates and is thus responsible for the collisional energy transfer.

The initial wave function (at time $t = 0$) corresponding to Equation(5.16) is

$$|\psi(0)\rangle = |\phi_i\rangle|\chi_j\rangle|\mathbf{P}_i, \mathbf{R}_i\rangle = |\phi_i\chi_j\mathbf{P}_i\mathbf{R}_i\rangle \tag{5.18}$$

where $\phi_i(\mathbf{q}_A)$ and $\chi_j(\mathbf{q}_B)$ are eigenfunctions of $\hat{h}_A$ and $\hat{h}_B$,

$$\hat{h}_A|\phi_i\rangle = E_i^A|\phi_i\rangle \tag{5.19a}$$

$$\hat{h}_B|\chi_j\rangle = E_j^B|\chi_j\rangle, \tag{5.19b}$$

and the translational wave function is a coherent state (*c.f.*, Equation(4.8)) with $|\mathbf{R}_i|$ large enough that A and B are non-interacting. The time-evolved wave function is given by,

$$|\psi(t)\rangle = e^{-i\hat{H}t/\hbar}|\psi(0)\rangle \tag{5.20}$$

so that the probability for molecule A to experience an energy transfer of $\Delta E_A = E_{i'}^A - E_i^A$ is given by

$$P_i(\Delta E_A) = \lim_{\bar{t}\to\infty} \sum_j \frac{e^{-\beta E_j^B}}{Q_B} \langle\psi(\bar{t})|\delta(\Delta E_A + E_i^A - \hat{h}_A)|\psi(\bar{t})\rangle. \tag{5.21}$$

The long time, $\bar{t} \to \infty$, entails a complete $A + B$ collision, and Equation(5.21) also includes a Boltzmann average over initial states of the bath molecule B, Q_B being its partition function,

$$Q_B = tr[e^{-\beta\hat{h}_B}]. \tag{5.22}$$

By using the Fourier representation of the delta function in Equation(5.21),

$$\delta(z) = (2\pi\hbar)^{-1} \int_{-\infty}^{\infty} dt\ e^{izt/\hbar}, \tag{5.23}$$

one obtains $P_i(\Delta E_A)$ as the Fourier transformation of a time correlation function,

$$P_i(\Delta E_A) = (2\pi\hbar)^{-1} \int_{-\infty}^{\infty} dt\ e^{i\Delta E_A t/\hbar} C_i(t), \tag{5.24a}$$

where the correlation function is

$$\begin{aligned} C_i(t) = \lim_{\bar{t}\to\infty} Q_B^{-1} \sum_j \\ \langle\phi_i\chi_j\mathbf{P}_i\mathbf{R}_i|e^{-\beta\hat{h}_B} e^{i\hat{h}_A t/\hbar} e^{i\hat{H}\bar{t}/\hbar} e^{-i\hat{h}_A t/\hbar} e^{-i\hat{H}\bar{t}/\hbar}|\phi_i\chi_j\mathbf{P}_i\mathbf{R}_i\rangle, \end{aligned} \tag{5.24b}$$

and the facts have been used that $|\phi_i\rangle$ and $|\chi_j\rangle$ are eigenstates of $\hat{h}_A$ and $\hat{h}_B$, respectively (*c.f.*, Equation(5.19a)).

At this point the forward-backward version of the SC-IVR is used for the product of time evolution operators in Equation(5.24b); they are all combined into *one* semiclassical step, given by the IVR of Equation(4.6),

$$e^{i\hat{h}_A t/\hbar} e^{i\hat{H}\bar{t}/\hbar} e^{-i\hat{h}_A t/\hbar} e^{-i\hat{H}\bar{t}/\hbar} = \tag{5.25}$$
$$(2\pi\hbar)^{-F} \int d\mathbf{p}_0 \int d\mathbf{q}_0 C_0(\mathbf{p}_0, \mathbf{q}_0) e^{iS_0(\mathbf{p}_0,\mathbf{q}_0)/\hbar} |\mathbf{p}_0', \mathbf{q}_0'\rangle \quad \langle \mathbf{p}_0, \mathbf{q}_0|.$$

The classical trajectory involved in the RHS of Equation(5.25) begins at time 0 with initial conditions $(\mathbf{p}_0, \mathbf{q}_0)$, evolves via the total classical Hamiltonian H until time $\bar{t}$, then to time $\bar{t}+t$ via the Hamiltonian h_A — *i.e.*, free motion of molecule A with the degrees of freedom of molecule B 'frozen' — then backwards in time to t via the total Hamiltonian H, and finally back to time 0 via the Hamiltonian h_A. $(\mathbf{p}_0', \mathbf{q}_0')$ are the final values from this trajectory which one may represent schematically as,

$$0 \xrightarrow{H} \bar{t} \xrightarrow{h_A} \bar{t}+t \xrightarrow{H} t \xrightarrow{h_A} 0. \tag{5.26}$$

The coordinates and momenta are all continuous at the various 'break times'; only the Hamiltonian is changed. The classical action S_0 and the pre-factor C_0 are given by,

$$S_0 = \int_0^{\bar{t}} dt' \; (\mathbf{p}\cdot\dot{\mathbf{q}} - H) + \int_{\bar{t}}^{\bar{t}+t} dt' \; (\mathbf{p}\cdot\dot{\mathbf{q}} - h_A) \tag{5.27a}$$
$$\int_{\bar{t}+t}^{t} dt' \; (\mathbf{p}\cdot\dot{\mathbf{q}} - H) + \int_t^0 dt' \; (\mathbf{p}\cdot\dot{\mathbf{q}} - h_A)$$

$$C_0 = \left| \frac{1}{2} \left(\frac{\partial \mathbf{q}_0'}{\partial \mathbf{q}_0} + \frac{\partial \mathbf{p}_0'}{\partial \mathbf{p}_0} - i\gamma\hbar \frac{\partial \mathbf{q}_0'}{\partial \mathbf{p}_0} + \frac{i}{\gamma\hbar} \frac{\partial \mathbf{p}_0'}{\partial \mathbf{q}_0} \right) \right|^{1/2}. \tag{5.27b}$$

Since the coherent states in Equation(5.25) have a direct product form, *e.g.*,

$$|\mathbf{p}_0, \mathbf{q}_0\rangle = |\mathbf{p}_0^A, \mathbf{q}_0^A\rangle |\mathbf{p}_0^B, \mathbf{q}_0^B\rangle |\mathbf{P}_0, \mathbf{R}_0\rangle, \tag{5.28}$$

and similarly for $|\mathbf{p}_0', \mathbf{q}_0'\rangle$, the time correlation function of Equation(5.24b) becomes

$$C_i(t) = Q_B^{-1} (2\pi\hbar)^{-F} \int d\mathbf{p}_0 \int d\mathbf{q}_0 \; C_0(\mathbf{p}_0, \mathbf{q}_0) e^{iS_0(\mathbf{p}_0,\mathbf{q}_0)/\hbar} \tag{5.29}$$
$$\langle \mathbf{p}_0^B \mathbf{q}_0^B | e^{-\beta\hat{h}_B} | \mathbf{p}_0'^B \mathbf{q}_0'^B \rangle \langle \mathbf{p}_0^A \mathbf{q}_0^A | \phi_i \rangle \langle \phi_i | \mathbf{p}_0'^A \mathbf{q}_0'^A \rangle \langle \mathbf{P}_0 \mathbf{R}_0 | \mathbf{P}_i \mathbf{R}_i \rangle \langle \mathbf{P}_i \mathbf{R}_i | \mathbf{P}_0' \mathbf{R}_0' \rangle,$$

with the limit $\bar{t}$ large.

Equation(5.29) is the basic theoretical result of FB-IVR for molecular energy transfer. It gives the correlation function (and the energy transfer probability via its Fourier transform, Equation(5.24a)) as a single phase space average over the initial conditions of classical trajectories that run forward and then backward as indicated via Equation(5.26). A significant advantage of the FB-IVR, beyond the reduction of the number of phase space integrals, is that the forward and backward contributions to S_0 in Equation(5.27a) should approximately cancel one another for small t and for molecular degrees of freedom which are weakly coupled. This cancelation leads a less oscillatory integrand. It would be most natural to evaluate this phase space average via Monte Carlo, with a sampling function corresponding to the $t = 0$ value of this integrand; since $(\mathbf{p}_0', \mathbf{q}_0') = (\mathbf{p}_0, \mathbf{q}_0)$ for $t = 0$ — *i.e.*, the backwards trajectory of Equation(5.26) exactly re-traces the forward trajectory — this Monte Carlo sampling function is

$$\rho(\mathbf{p}_0, \mathbf{q}_0) = \langle \mathbf{p}_0^B \mathbf{q}_0^B | e^{-\beta \hat{h}_B} | \mathbf{p}_0^B \mathbf{q}_0^B \rangle \left| \langle \mathbf{p}_0^A \mathbf{q}_0^A | \phi_i \rangle \right|^2 |\langle \mathbf{P}_0 \mathbf{R}_0 | \mathbf{P}_i \mathbf{R}_i \rangle|^2 , \tag{5.30}$$

which is recognized as the Husimi distribution[120] for the initial state and is therefore a most reasonable choice. Also, in many cases one expects only short values of the time t to be necessary to obtain $P_i(\Delta E_A)$; *e.g.*, if the energy transfer probability were of the Gaussian form as in Equation(5.14b), then the correlation function would also be Gaussian,

$$C_i(t) = \int_{-\infty}^{\infty} d\Delta E_A \; e^{-i\Delta E_A t/\hbar} P_i(\Delta E_A) \propto e^{-\Delta^2 t^2/4\hbar^2} . \tag{5.31}$$

In three dimensional collision systems one is actually interested in the *cross section*, which can be obtained from the probability $P_i(\Delta E_A)$ in the usual way. One can without restriction choose the translational momentum vector $\mathbf{P}_i$ as the z-axis

$$\mathbf{P}_i = (0, 0, P_i) \tag{5.32a}$$

and then parametrize the initial translational coordinate via an impact parameter b, and azimuthal angle ϕ

$$\mathbf{R}_i = (bcos\phi, bsin\phi, -\sqrt{R_{max}^2 - b^2}) \tag{5.32b}$$

where R_{max} is a value large enough for A and B to be non-interacting. The cross section for molecular energy transfer ΔE_A is then given by the angle and impact parameter average of the probability

$$\sigma_i(\Delta E_A) = \int_0^\infty db\, b \int_0^{2\pi} d\phi P_i(\Delta E_A). \tag{5.33}$$

(The average can be carried out on the correlation function $C_i(t)$ itself, so that $\sigma_i(\Delta E_A)$ is then given by the Fourier transform of this impact parameter averaged time correlation function.) If one furthermore averages over a Boltzmann distribution of translational energies, one obtains a rate constant for energy transfer,

$$\begin{aligned} k_i(\Delta E_A) &\equiv \langle \tfrac{P_i}{\mu} \sigma_i(\Delta E_A) \rangle \\ &= (\tfrac{8\kappa T}{\pi\mu})^{1/2} \textstyle\int_0^\infty d(\tfrac{E_t}{\kappa T})\, \tfrac{E_t}{\kappa T} e^{-E_t/\kappa T} \sigma_i(\Delta E_A) \end{aligned} \tag{5.34}$$

where $E_t = P_i^2/2\mu$.

Finally, we note the simplifications that occur if the bath gas B is atomic, *i.e.*, has no internal degrees of freedom. The coordinates $(\mathbf{p}_B, \mathbf{q}_B)$ do not enter, the Hamiltonian $\hat{h}_B \longrightarrow 0$, and the factors in Equation(5.29) involving these degrees of freedom become unity, *i.e.*,

$$Q_B^{-1} \langle \mathbf{p}_0^B \mathbf{q}_0^B | e^{-\beta \hat{h}_B} | \mathbf{p}_0'^B \mathbf{q}_0'^B \rangle \longrightarrow 1 \tag{5.35}$$

5.5.2 Translation Energy Distribution

In some applications one may be more interested in the energy gained (or lost) from the translational degrees of freedom than from the internal degrees of freedom

of molecule A. This is most common if molecule A is an atom; the bath species B may be a molecule or even a more complex substrate, *e.g.*, a solid or surface or a molecular cluster. In this case one is interested in the probability distribution of the translational energy after atom A collides with the molecule (or substrate) B, and the appropriate modification of Equation(5.21) is

$$P_{tr}(\Delta E) = \lim_{\bar{t}\to\infty} \sum_j \frac{e^{-\beta E_j^B}}{Q_B} \langle\psi(\bar{t})|\delta(\Delta E + \frac{P_i^2}{2\mu} - \frac{\hat{P}^2}{2\mu})|\psi(\bar{t})\rangle. \tag{5.36}$$

Here the initial state is

$$|\psi(0)\rangle = |\chi_j\rangle|\mathbf{P}_i\mathbf{R}_i\rangle, \tag{5.37}$$

since atom A has no internal degrees of freedom. Proceeding in a similar manner as from Equation(5.21) to Equation(5.29) gives an analogous result,

$$P_{tr}(\Delta E) = \frac{1}{2\pi\hbar}\int_{-\infty}^{\infty} dt\ e^{i\Delta E t/\hbar} C_{tr}(t) \tag{5.38a}$$

with the correlation function given by

$$\begin{aligned} C_{tr}(t) = Q_B^{-1}(2\pi\hbar)^{-F} \int d\mathbf{p}_0 \int d\mathbf{q}_0\ C_0(\mathbf{p}_0, \mathbf{q}_0) e^{iS_0(\mathbf{p}_0,\mathbf{q}_0)/\hbar} \\ \langle \mathbf{p}_0^B \mathbf{q}_0^B | e^{-\beta\hat{h}_B} | \mathbf{p}_0'^B \mathbf{q}_0'^B\rangle \langle \mathbf{P}_0\mathbf{R}_0|\mathbf{P}_i\mathbf{R}_i\rangle\langle \mathbf{P}_i\mathbf{R}_i|\mathbf{P}_0'\mathbf{R}_0'\rangle. \end{aligned} \tag{5.38b}$$

Here the forward-backward trajectory is that indicated schematically by,

$$0 \xrightarrow{H} \bar{t} \xrightarrow{\mathbf{P}^2/2\mu} \bar{t}+t \xrightarrow{H} t \xrightarrow{\mathbf{P}^2/2\mu} 0, \tag{5.39}$$

i.e., in the $\bar{t} \longrightarrow \bar{t}+t$ and $t \longrightarrow 0$ time intervals the propagation is generated by the Hamiltonian $\mathbf{P}^2/2\mu$, *i.e.*, free particle evolution of the translation degree of freedom with the internal degrees of freedom of B 'frozen'. The full Hamiltonian H governs the trajectory during the time intervals $0 \longrightarrow \bar{t}$ and $\bar{t}+t \longrightarrow t$. The forward-backward action integral is thus given by,

$$S_0 = \begin{array}{l} \int_0^{\bar{t}} dt' \, (\mathbf{p} \cdot \dot{\mathbf{q}} - H) + \frac{\mathbf{P}_i^2}{2\mu} t \\ \int_{\bar{t}+t}^{t} dt' \, (\mathbf{p} \cdot \dot{\mathbf{q}} - H) - \frac{\mathbf{P}_f^2}{2\mu} t \end{array} \tag{5.40}$$

and the pre-factor $C_0(\mathbf{p}_0, \mathbf{q}_0)$ has the same form as before.

5.6 Application to $He + H_2(v_i) \rightarrow He + H_2(v_f)$

We apply the formalism developed above to the well studied Secrest-Johnson[68] model of vibrationally inelastic scattering. The Hamiltonian for the collision system is

$$H(P, R, p, q) = \frac{P^2}{2\mu} + h_A(p, q) + V(R, q), \tag{5.41}$$

where (p, q) and (P, R) are the vibrational and translational respectively. The internal Hamlitonian and interaction potential are,

$$h_A(p, q) = \frac{p^2}{2m} + \frac{1}{2} m\omega^2 q^2, \tag{5.42a}$$

$$V(R, q) = e^{\alpha(q-R)}, \tag{5.42b}$$

and $h_B = 0$ since He has no internal degrees of freedom. In the reduced units used by Secrest and Johnson, $m = 1, \omega = 1, \alpha = 0.3$, and $\mu = 2/3$ for the $He + H_2$ system. Written in this way, we are considering the molecular system H_2 (molecule A in the previous section) to exchange energy via collision with the Helium bath system (molecule B).

The initial state of the total system is

$$|\psi_i\rangle = |P_i, R_i\rangle |\phi_i\rangle, \tag{5.43a}$$

with

$$\hat{h}_A|\phi_i\rangle = (v_i + 1/2)\hbar\omega|\phi_i\rangle. \tag{5.43b}$$

We calculate the energy transfer distribution $P_i(\Delta E_A)$ for a fixed total energy. This microcanonical calculation, as opposed to the thermal formalism developed in the previous section, allows us to compare our results to previous SC-IVR and quantum state-resolved work. The extension to a Boltzmann distribution of kinetic energies (*c.f.*, Equation(5.29)) is straightforward. For fixed total energy, E, the energy transfer distribution $P_i(\Delta E_A)$ is given by

$$P_i(\Delta E_A) = \int_{-\infty}^{\infty} dt\ e^{i\Delta E_A t/\hbar} C_i(t), \tag{5.44}$$

where the correlation function is given by Equation(5.29) (with $\hat{h}_B \equiv 0$),

$$\begin{aligned} C_i(t) = (2\pi\hbar)^{-2} \int dp_0\ dq_0\ \int dP_0\ dR_0\ C_0(\mathbf{p}_0, \mathbf{q}_0) e^{iS_0(\mathbf{p}_0,\mathbf{q}_0)/\hbar} \\ \langle p_0' q_0'|\phi_i\rangle\langle\phi_i|p_0 q_0\rangle\langle P_0' R_0'|P_i R_i\rangle\langle P_i R_i|P_0 R_0\rangle \end{aligned} \tag{5.45}$$

The total energy $E = P_i^2/2\mu + (v_i + 1/2)\hbar\omega$ is well defined if the initial coherent state $|P_i, R_i\rangle$ is sufficiently broad that it approximates a plane wave. We choose $\gamma_R = 0.2$ and $R_i = 80$ to ensure that this is so ($\langle(\Delta P_i)^2\rangle = 0.1$). γ_q is chosen to be the natural width for the oscillator coordinate $m\omega/\hbar$. The phase space average of over initial conditions is evaluated by Monte Carlo using the Sobol deterministic space filling sequence[76]. (p_0', q_0', P_0', R_0') are the final coordinates and momenta resulting from the forward-backward trajectory indicated by Equation(5.26), and the monodromy matrix elements necessary for construction of the prefactor $C_0(\mathbf{p}_0, \mathbf{q}_0)$ (*c.f.*Equation(4.7)) were computed by integration of the auxillary equations of motion as usual([51]).

5.7 FB-IVR Results

Figure 5.6 shows the time correlation function given by the FB-IVR procedure, *i.e.*, Equation(5.45), and also the exact quantum (QM) result,

$$C_i^{QM}(t) = \sum_j P_{v_j,v_i}(E) e^{-i\omega(v_j - v_i)t}, \tag{5.46}$$

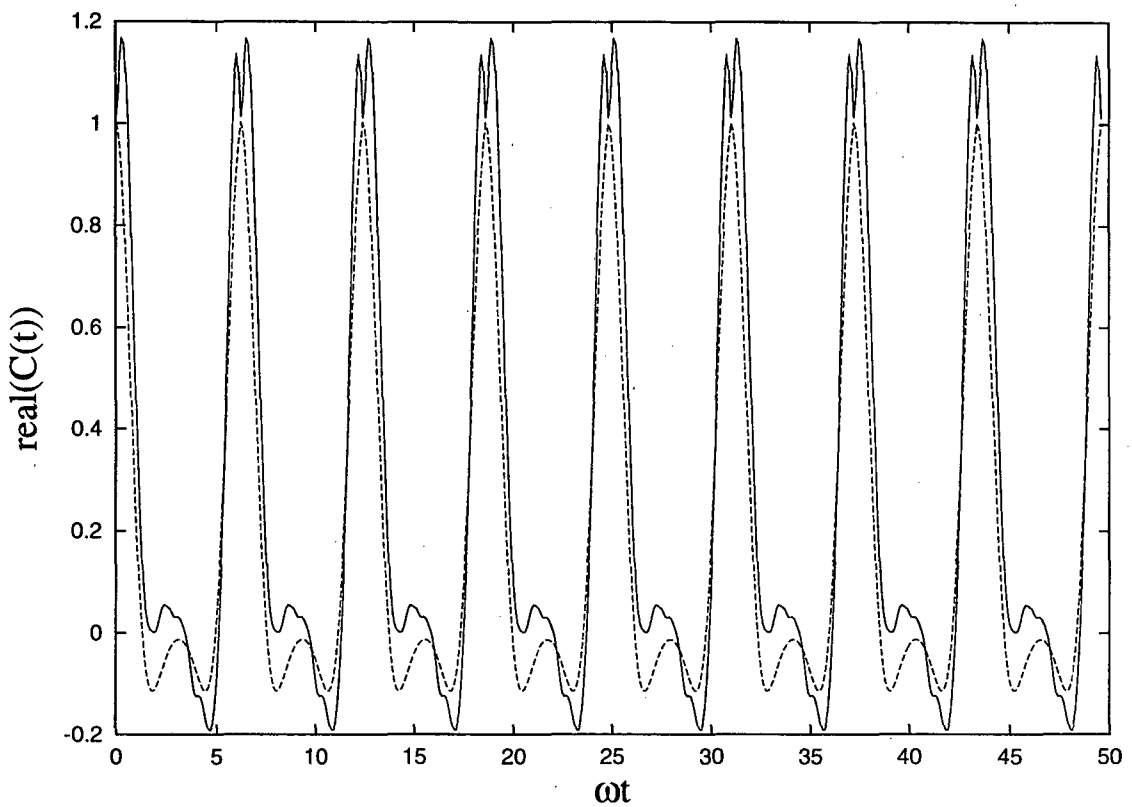

Figure 5.6: A comparison of the exact quantum correlation function (dotted line) and the semiclassical one (solid line) computed using Equation(5.45).

where $\{P_{v_j,v_i}\}$ are the QM transition probabilities for the $v_i \rightarrow v_j$ inelastic transition. The correlation functions show much more structure than the simple behavior suggested in Equation(5.31), this being due to the widely spaced vibrational energy levels of H_2 (molecule A in this example). The vibrational levels in a highly excited polyatomic molecule will typically form a near continuum and thus considerably quench this pronounced oscillatory structure. The present example is thus a severe test of the extent to which the FB-IVR model can describe quantum coherence effects in molecular energy transfer.

There is reasonable agreement between the FB-IVR and QM correlation functions in Figure 5.6, but the more important comparison is their Fourier transforms, *i.e.*, $P_i(\Delta E_A)$.

Figure 5.7 shows the FB-IVR result for $P_i(\Delta E_A)$ for several initial states and total

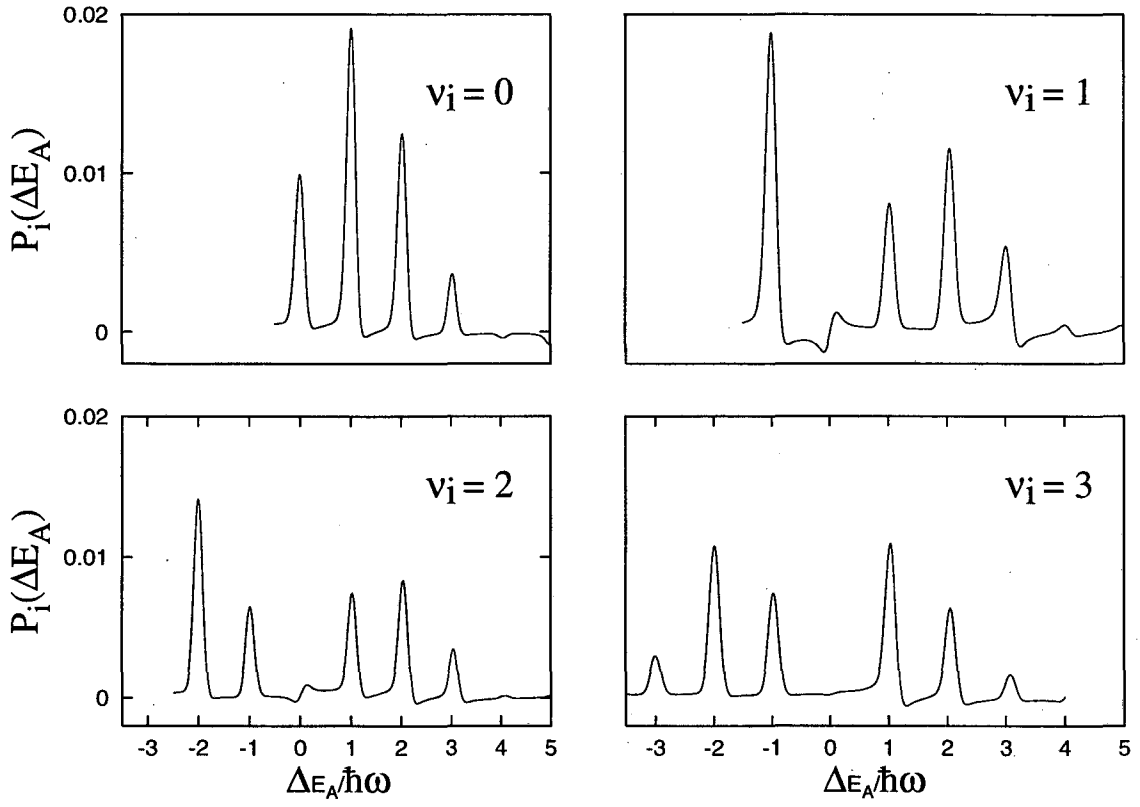

Figure 5.7: Energy Transfer Spectra (E=8.0) using the FB-IVR Equation(5.24a)

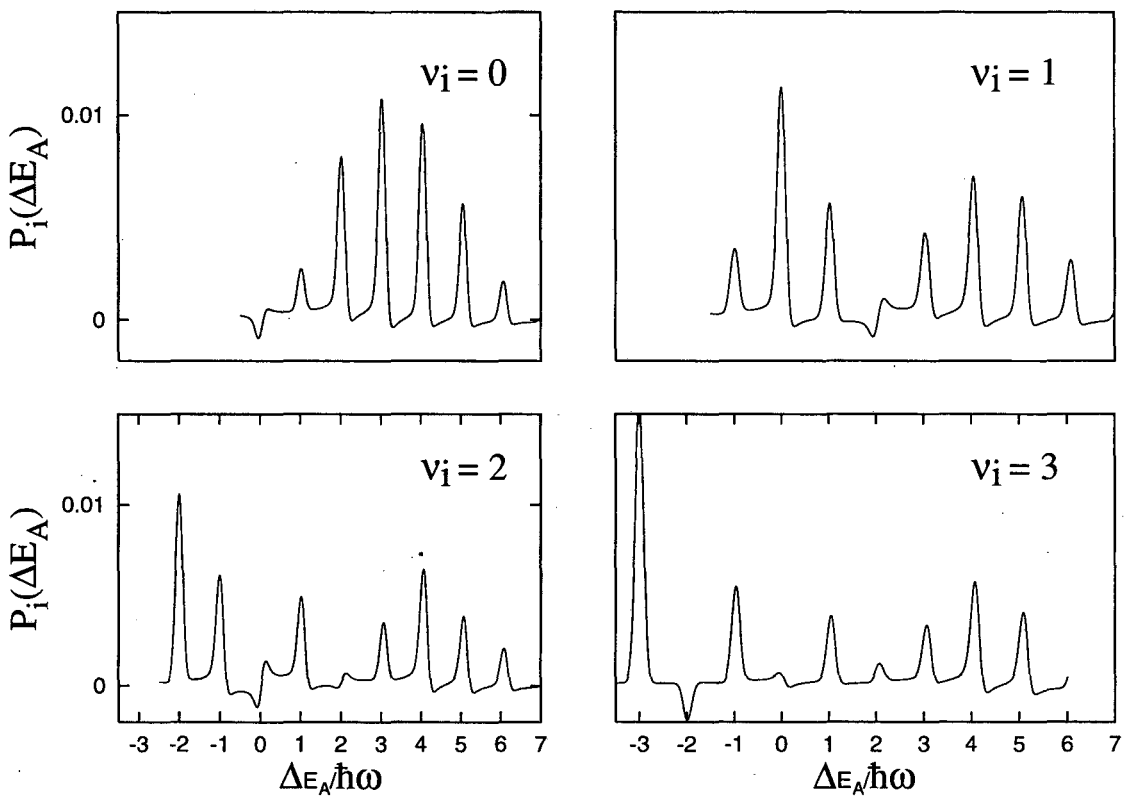

Figure 5.8: Energy Transfer Spectra (E=12.0) using the FB-IVR Equation(5.24a)

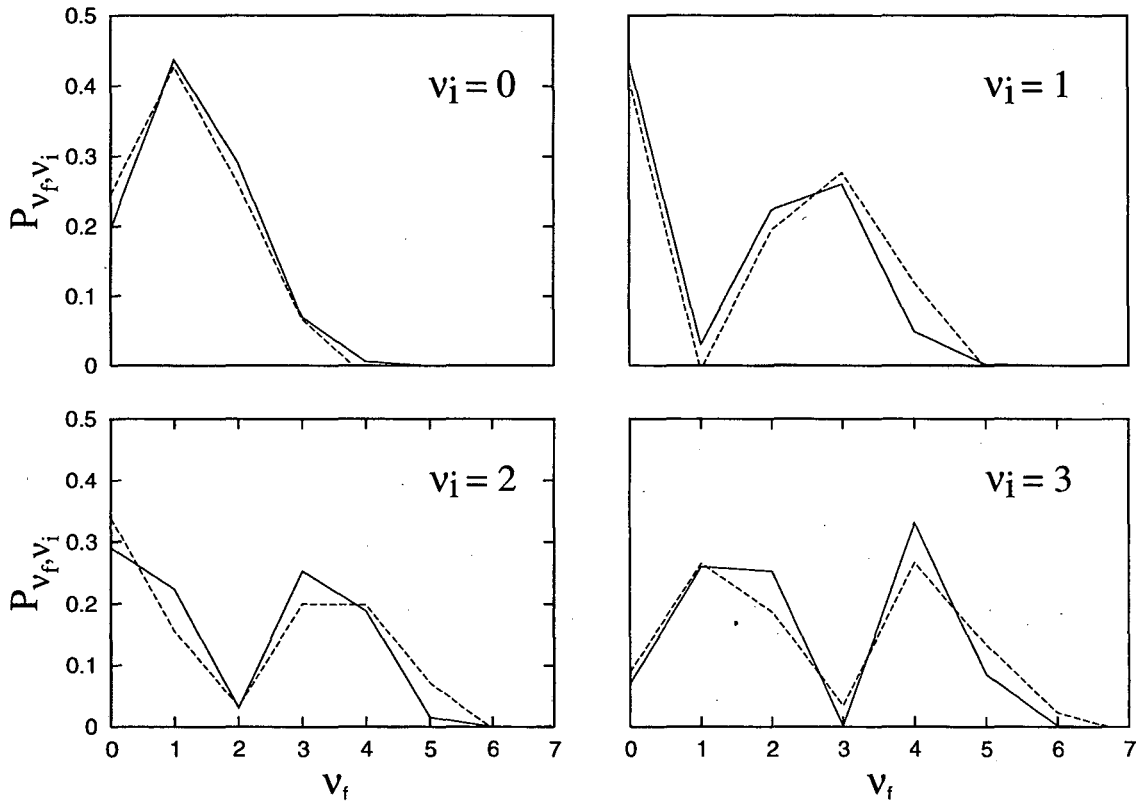

Figure 5.9: Vibrational transition probabilities as a function of final vibrational quantum number v_f, for several initial vibrational states v_i, and total energy $E = 8.0$. The solid lines connect the exact quantum values, and the dashed lines are those given by the FB-IVR, Equation(5.15). The values correspond to the integrated area of the peaks in Figure(5.7).

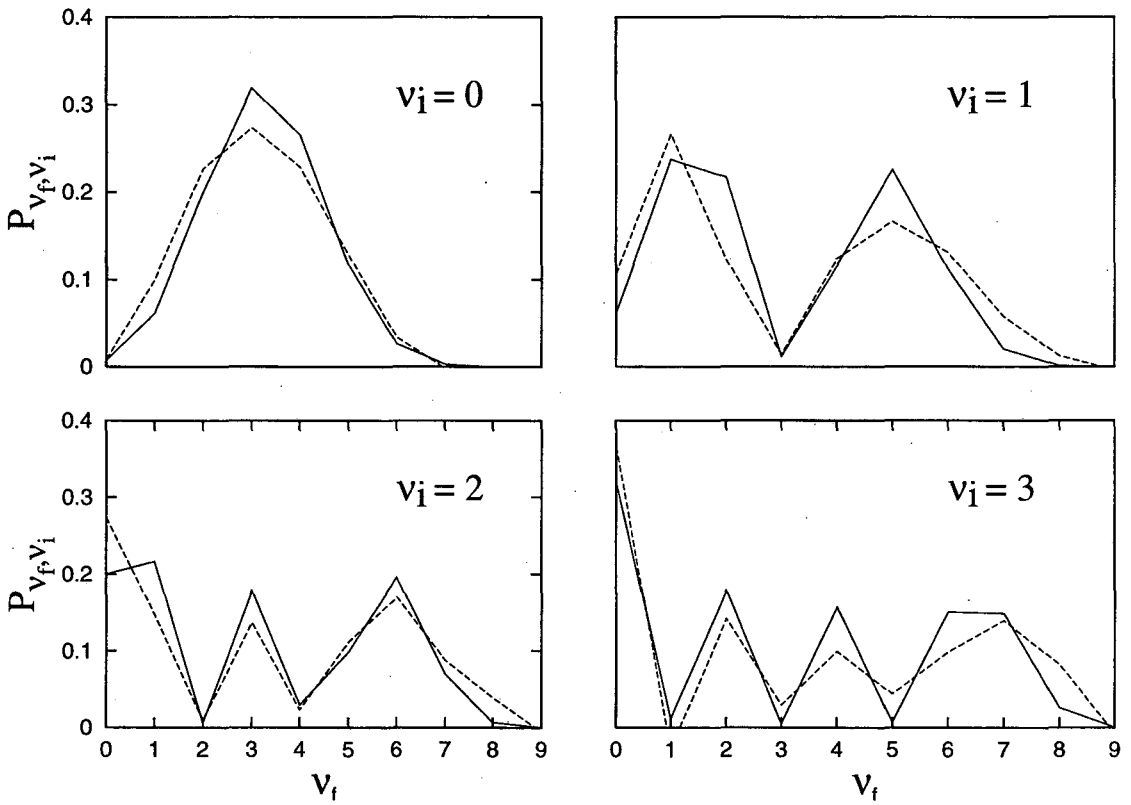

Figure 5.10: Vibrational transition probabilities as a function of final vibrational quantum number v_f, for several initial vibrational states v_i, and total energy $E = 12.0$. The solid lines connect the exact quantum values, and the dashed lines are those given by the FB-IVR, Equation(5.15). The values correspond to the integrated area of the peaks in Figure(5.8).

energies, and the exact QM result is given by

$$P_i^{QM}(\Delta E_A) = \sum_j P_{v_j,v_i}(E)\delta(\Delta E_A - \hbar\omega(v_j - v_i)) \tag{5.47}$$

The peaks in Figure 5.7 have finite width because of the finite energy spread in the initial translational coherent state $|P_i, R_i\rangle$ and also because of the finite time used in computing the Fourier transform of $C_i(t)$. Here, too, the quantized structure of the H_2 vibrational states dominates the picture; for a polyatomic molecule A one would have a dense set of peaks (essentially overlapping) and thus expect to see results for $P_i(\Delta E_A)$ closer to the qualitative form of Equation(5.14). Again, this highly quantized nature of the H_2 vibrational states provides a good test of how well the FB-IVR approach can describe such quantum effects.

The most definite comparison of the FB-IVR and QM results is achieved by integrating to obtain the area under the peaks in Figure 5.7 and identifying these with the individual quantum transition probabilities $\{P_{v_j,v_i}\}$. This comparison is shown in Figure 5.10. The oscillatory structure in $\{P_{v_j,v_i}\}$ versus v_j — *i.e.*, the product state distribution— is well-understood from the earlier classical S-matrix treatment[102] of this system as arising from the interference of two classical trajectories that emerge from the stationary phase approximation to the IVR integral over initial conditions. Our previous IVR study of this system has shown[111] that a the full HK-IVR treatment accurately describes this interference structure. Here we see that the FB-IVR approach also gives reasonably good results, though somewhat less accurate than the full HK-IVR treatment.

We also carried out the calculation of $P_i(\Delta E_A)$ treating the He atom as the molecular system and H_2 as the 'substrate', *i.e.*using the formulation in Section 5.5.1. The results are essentially the same as the above FB-IVR, though it is more efficient to treat H_2 as the molecular system since it requires shorter trajectories.

The Monte Carlo evaluation of Equation(5.45) for a particular value of t requires a rather modest 5000 trajectories for convergence. However the present method requires a distinct trajectory for each time point in the correlation function, so the overall computational effort is comparable to a full HK-IVR calculation. For larger systems with more modes for energy transfer we expect the correlation function to die off

more rapidly and the spectrum to be broadened more than in the present highly coherent example. For systems which less oscillatory correlation functions we expect the FB-IVR to be even more efficient.

The purpose of this section has been to show how the forward-backward version of the semiclassical IVR can be used to obtain molecular energy transfer probabilities, and to provide a numerical test to see how well it can describe the quantum effects therein. We find that the FB-IVR gives reasonably accurate results for the Secrest-Johson model of inelastic scattering. For larger molecular systems it should be even more efficient (compared to a full state-to-state calculation) since the high vibrational state density should cause the time correlation function to decay more rapidly.

5.8 FB-IVR for Larger Systems

In some applications involving large molecules A one is interested not in the dependence of the energy transfer probability on the individual initial *state* of molecule A, but rather only its dependence on the initial internal *energy* of molecule A. If E denotes the initial internal energy of molecule A, and E' its final internal energy (*i.e.*, $\Delta E_A = E' - E$), then this quantity — usually denoted $P(E' \leftarrow E)$ — is given by averaging $P_i(\Delta E_A)$ over a microcanonical distribution of initial states all having energy E,

$$P(E' \leftarrow E) = \sum_i \delta(E - E_i^A) P_i(E' - E)/\rho_A(E), \tag{5.48}$$

where $\rho_A(E) = \sum_i \delta(E - E_i^A)$ is the microcanonical density of states of molecule A. Using Equation(5.29) for $P_i(E' - E) \equiv P_i(\Delta E_A)$ thus gives,

$$\begin{aligned} P(E' \leftarrow E) = \frac{1}{Q_B \rho_A(E)} \sum_i \delta(E - E_i^A) \int_{-\infty}^{\infty} dt' \; e^{i(E'-E)t'/\hbar} \\ \langle \phi_i \chi_j \mathbf{P}_i, \mathbf{R}_i | e^{-\beta \hat{h}_B} e^{i\hat{h}_A t'/\hbar} e^{i\hat{H}\bar{t}/\hbar} e^{-i\hat{h}_A t'/\hbar} e^{-i\hat{H}\bar{t}/\hbar} | \phi_i \chi_j \mathbf{P}_i \mathbf{R}_i \rangle. \end{aligned} \tag{5.49}$$

Proceeding as before, one can use the Fourier representation of the delta function in Equation(5.23), so that this 'energy-to-energy' transition probability is given by a

two-dimensional Fourier transform,

$$P(E' \leftarrow E) = (2\pi\hbar)^{-2} \int_{-\infty}^{\infty} dt \int_{-\infty}^{\infty} dt' e^{i(E't'-Et)/\hbar} C(t,t') \tag{5.50}$$

with the two time correlation function given by

$$C(t',t) = \frac{1}{Q_B \rho_A(E)} tr\left(|\mathbf{P}_i\mathbf{R}_i\rangle\langle\mathbf{P}_i\mathbf{R}_i| e^{-\beta\hat{h}_B} e^{i\hat{h}_A t/\hbar} e^{i\hat{H}\bar{t}/\hbar} e^{-i\hat{h}_A t'/\hbar} e^{-i\hat{H}\bar{t}/\hbar}\right), \tag{5.51}$$

with $\bar{t}$ large.

The FB-IVR treatment of this two dimensional correlation function leads to trajectories which evolve via the following forward and backward steps,

$$0 \xrightarrow{H} \bar{t} \xrightarrow{h_A} \bar{t} + t' \xrightarrow{H} t' \xrightarrow{h_A} t' - t. \tag{5.52}$$

The FB-IVR evaluation of Equation(5.51) involves only coherent state overlaps and thus the energy eigenstates of A need not be calculated. Additionally, we expect the practical benefit that for small energy transfers, $E' - E$, $C(t',t)$ should be small except for $t \simeq t'$.

Table 5.1: Molecular Energy Transfer Probabilities for $H_2(\nu) + He \rightarrow H_2(v') + He$ $(E = 8.0)$

ν, v'	HK-IVR	LSC-IVR	FB-IVR	Exact
0,0	0.2093	0.1967	0.2436	0.1978
0,1	0.4363	0.4230	0.4269	0.4367
0,2	0.2732	0.3101	0.2626	0.2905
0,3	0.0710	0.0748	0.0669	0.0699
0,4	0.0086	-0.0015	-0.0192	0.0056
0,5	0.0003	-0.0016	-0.0200	0.0001
0,6	0.0000	-0.0006	-0.0035	0.0000
0,7	0.0000	0.0003	-0.0022	0.0000
1,0	0.4122	0.4217	0.4861	0.4367
1,1	0.0282	0.0692	0.0497	0.0302
1,2	0.2323	0.1553	0.1785	0.2237
1,3	0.2364	0.2910	0.2467	0.2602
1,4	0.0521	0.0620	0.0871	0.0491
1,5	0.0089	-0.0123	0.0014	0.0017
1,6	0.0007	0.0023	-0.0008	0.0000
1,7	0.0009	-0.0002	-0.0033	0.0000
2,0	0.2842	0.2943	0.3433	0.2905
2,1	0.2138	0.1839	0.1559	0.2237
2,2	0.0316	0.0890	0.0385	0.0305
2,3	0.2701	0.1518	0.1998	0.2531
2,4	0.1837	0.2500	0.1952	0.1889
2,5	0.0252	-0.0030	0.0665	0.0153
2,6	0.0027	-0.0007	-0.0015	0.0002
2,7	0.0016	0.0018	0.0009	0.0000
3,0	0.0717	0.0734	0.0874	0.0699
3,1	0.2659	0.2859	0.2641	0.2602
3,2	0.2746	0.1777	0.1908	0.2531
3,3	0.0030	0.0290	0.0343	0.0015
3,4	0.3064	0.2741	0.2689	0.3310
3,5	0.0823	0.1406	0.1282	0.0849
3,6	0.0098	-0.0094	0.0261	0.0018
3,7	0.0013	0.0032	-0.0070	0.0000

Table 5.2: Molecular Energy Transfer Probabilities for $H_2(\nu) + He \rightarrow H_2(v') + He$ ($E = 12.0$)

ν, v'	HK-IVR	LSC-IVR	FB-IVR	Exact
0,0	0.0063	0.0097	0.0080	0.0074
0,1	0.0652	0.0647	0.1002	0.0616
0,2	0.2031	0.1866	0.2269	0.2002
0,3	0.3196	0.2996	0.2736	0.3188
0,4	0.2593	0.2823	0.2286	0.2653
0,5	0.1076	0.1442	0.1286	0.1170
0,6	0.0230	0.0231	0.0341	0.0266
0,7	0.0029	-0.0096	-0.0016	0.0028
1,0	0.0560	0.0647	0.1061	0.0616
1,1	0.2383	0.2150	0.2664	0.2372
1,2	0.2118	0.2286	0.1230	0.2168
1,3	0.0105	0.0608	0.0138	0.0113
1,4	0.1170	0.0516	0.1237	0.1156
1,5	0.2243	0.2022	0.1662	0.2255
1,6	0.0998	0.1726	0.1310	0.1117
1,7	0.0188	0.0229	0.0576	0.0202
2,0	0.1820	0.1863	0.2736	0.2002
2,1	0.2188	0.2322	0.1472	0.2168
2,2	0.0066	0.0363	0.0099	0.0059
2,3	0.1840	0.1096	0.1368	0.1784
2,4	0.0319	0.1241	0.0233	0.0294
2,5	0.0972	0.0178	0.1119	0.0987
2,6	0.2056	0.1627	0.1703	0.1958
2,7	0.0652	0.1485	0.0878	0.0698
3,0	0.3137	0.3247	0.3663	0.3188
3,1	0.0096	0.0242	-0.0289	0.0113
3,2	0.1875	0.1294	0.1419	0.1784
3,3	0.0064	0.0870	0.0294	0.0047
3,4	0.1716	0.0582	0.0992	0.1568
3,5	0.0053	0.1467	0.0438	0.0069
3,6	0.1674	0.0320	0.0982	0.1506
3,7	0.1670	0.1594	0.1393	0.1486

Chapter 6

Summary and Conclusions

This work has developed quantum mechanical and semiclassical methods which describe chemical dynamics and bring physically useful quantities within reach of calculation. The calculations of we are capable of completing really depend on two things. The first is our ability to come up with insightful and efficient expressions for the physical quantities of interest. Second are the algorithms and computer equipment to carry out the calculations. A lack of the first can be overcome with more of the second, but will never keep up with a good dose of both. Here we examine future directions for both of these ingredients of chemical physics research.

The dimensional scaling problem with the direct quantum mechanical methods we have discussed can be treated by methods which implement more intelligent, and albeit more complicated basis sets. Wavelet[124] or multiresolution[125] methods provide grid methods which place a greater density of basis functions in regions where they are needed ,*i.e.*, where kinetic energy is large. In our case of HO_2 the dynamics within the collision complex well would benefit from these methodologies.

Another approach to beating the N^d scaling is the use of time dependent basis sets. Multiconfiguration time dependent Hartree[122](MCTDH) and moving finite element[123] methods both attempt to put the basis set in the right place at the right time. Indeed at the time of this writing preliminary results on a 12 dimensional MCTDH thermal rate calculation[128] have been reported. Finite element methods are commonly accepted as a standard tool for time dependent PDE's in other fields, *e.g.*,

computational fluid dynamics. Moving finite element methods span a wide range of implementations though their use in chemical reaction dynamics so far has been limited. There remains much to explore on these fronts.

The fundamental remaining problem with the semiclassical methods discussed is the oscillatory nature of the integrand. This problem surfaces in many different areas of science where Monte Carlo integration methods are implemented and hopefully the lessons learned between fields will be mutual. The FB-IVR integrand has been shown[88] to be much smoother than that of the SC-IVR. Likewise, Filinov smoothing, ergodic averaging[126,127], WKB like approximations to the prefactor, and adaptive and stratified sampling methods afford some help in this regard. The reason for trying to beat the oscillatory integrand problem by means other than brute force becomes particularly clear when one considers chaotic motion. Here the oscillations in the integrand can become larger than numbers easily represented on a computer. Thus we should avoid trying to beat the oscillatory integrand problem by brute force and instead pursue IVR approaches which avoid the need for summing an excessive number of contributions to reach any result.

For large systems the Herman Kluk SC-IVR is expected to experience a bottleneck in the calculation of the semiclasscal prefactor. The determinant in Equation(4.7) is a N^3 operation which presents, for large N, a significant computational effort. Approximate methods for surmounting this problem include the Log-Derivative integration methods and WKB like approximations to the prefactor.

SC-IVR approaches are a burgeoning research area and there remain many ideas yet to be explored on the semiclassical front.

Two future directions in scientific computing relevant to the present work are and distributed and quantum computing. Today the worlds largest supercomputers are clusters of workstations with fast network interconnects between nodes. This situation is distinctly different from 10 years ago when large vector computers were designed specifically for scientific research. Distributed scientific computation holds many promises and certainly a few challenges. While the compute power of individual CPUs increases at eighty percent a year, the aggregate compute power of a a cluster is not limited by this growth rate. However, since quantum mechanics is

inherently nonlocal, distributed scientific computing would benefit from new methods and algorithms which minimize the required communication between nodes. Finally quantum computers[129], though not yet implemented, are in theory ideally suited to direct quantum mechanical calculation.

In conclusion, a detailed understanding of the dynamics of molecules is important to many areas of the sciences. Bringing quantum mechanics, our best theory, together with molecular dynamics, our most readily applied theory, should prove to be both an enlightening and tremendously useful endeavor.

References

[1] W.H. Miller, S.D. Schwartz, and J.W. Tromp, *J. Chem. Phys.* **79**, 4889 (1983).

[2] (a) J.A. Jr. Fleck, J.R. Morris, and M.D. Feit, *Appl. Phys.* **10**, 129 (1976). (b) M.D. Feit, J.A. Fleck Jr., A. Steiger, *J. Comput. Phys.* **47**, 412 (1982).

[3] T. C. Germann and W. H. Miller, *J. Phys. Chem. A* **101**, 6358 (1997)

[4] M. J. Pilling and P. W. Seakins, *Reaction Kinetics*; (Oxford U. P. Oxford, 1995) Chapter 10.

[5] P. O. Wennberg, R. C. Cohen, R. M. Stimpfle, J. P. Koplow, J. G. Anderson, R. J. Salawitch, D. W. Fahey, E. L. Woodbridge, E. R. Keim, R. S. Gao, C. R. Webster, R. D. May, D. W. Toohey, L. M. Avallone, M. H. Proffitt, M. Lowenstein, J. R. Podolske, K. R. Chan, and S. C. Wofsy, *Science* **1994**, *266*, 398.

[6] W. C. Gardiner, *Combustion Chemistry* (Springer, Berlin FRG, 1984)

[7] J.A. Miller, R.J. Kee and C.K. Westbrook, *Annu. Rev. Phys. Chem.* **41**, 345 (1990).

[8] J.A. Miller, *J. Chem. Phys.* **84**, 6170 (1986).

[9] R. J. Duchovic, J. D. Pettigrew, B. Welling, and T. Shipchandler, *J. Chem. Phys.* **105**, 10367 (1996).

[10] (a) R.T. Pack, E.A. Butcher, and G.A. Parker, *J. Chem. Phys.* **99**, 9310 (1993). (b) R.T. Pack, E.A. Butcher, and G.A. Parker, *J. Chem. Phys.* **102**, 5998 (1995).

[11] (a) D.H. Zhang and J.Z.H. Zhang, *J. Chem. Phys.* **101**, 3671 (1994). (b) J. Dai and J.Z.H. Zhang, *J. Chem. Phys.* **104**, 3664 (1996). (c) J. Dai and J.Z.H. Zhang, *J. Phys. Chem.* **100**, 6898 (1996).

[12] C. Leforestier, and W.H. Miller, *J. Chem. Phys.* **100**, 733 (1994).

[13] (a) A.J. Dobbyn, M. Stumpf, H.-M. Keller, W.L. Hase, and R. Schinke, *J. Chem. Phys.* , **102**, 5867 (1995) (b) K. Song, G.H. Peslherbe, W.L. Hase, A.J. Dobbyn, M. Stumpf, and R. Schinke, *J. Chem. Phys.* **103**, 8891 (1995). (c) A.J. Dobbyn, M. Stumpf, H.-M. Keller, and R. Schinke, *J. Chem. Phys.* **103**, 9947 (1995). (d) A.J. Dobbyn, M. Stumpf, H.-M. Keller, and R. Schinke, *J. Chem. Phys.* **104**, 8357 (1996).

[14] X.T. Wu and E.F. Hayes, *J. Chem. Phys.* **107**, 2705 (1997).

[15] V.A. Mandelshtam, T.P. Grozdanov, and H.S. Taylor, *J. Chem. Phys.* **103**, 10074 (1995).

[16] J.M. Bowman, *J. Phys. Chem.* **95**, 4960 (1991).

[17] A. Meijer and E. Goldfield pre-print.

[18] H. Wang, W.H. Thompson, and W.H. Miller, *J. Chem. Phys.* **107**, 7194 (1997).

[19] T. Yamamoto, *J. Chem. Phys.* **33**, 281 (1960).

[20] W.H. Thompson and W.H. Miller, *J. Chem. Phys.* **102**, 9205 (1995).

[21] W.H. Thompson and W.H. Miller, *J. Chem. Phys.* **106**, 142 (1997).

[22] T.J. Park and J.C. Light, *J. Chem. Phys.* **88**, 4897 (1988).

[23] F. Matzkies and U. Manthe, *J. Chem. Phys.* (submitted).

[24] C. Lanczos, *J. Res. Natl. Bur. Stand.* **45**, 255 (1950).

[25] T.J. Park and J.C. Light, *J. Chem. Phys.* **88**, 4897 (1988).

[26] T. Seideman and W.H. Miller, *J. Chem. Phys.* **95**, 1768 (1991).

[27] D.G. Truhlar and B.C. Garrett, *Annu. Rev. Phys. Chem.* **35**, 159 (1984).

[28] (a) J.V. Lill, G.A. Parker, and J.C. Light, *Chem. Phys. Lett.* **89**, 483 (1982). (b) J.C. Light, I.P. Hamilton, and J.V. Lill, *J. Chem. Phys.* **82**, 1400 (1985). (c) J.V. Lill, G.A. Parker, and J.C. Light, *J. Chem. Phys.* **1986**, *85*, 900. (d) Z. Bačić, and J.C. Light, *J. Chem. Phys.* **1986**, *85*, 4594. (e) R.M. Whitnell and J.C. Light, *J. Chem. Phys.* **1988**, *89*, 3674. (f) S.E. Choi and J.C. Light, *J. Chem. Phys.* **1990**, *92*, 2129.

[29] The symmetry requirements of the HO_2 wavefunction are discussed more fully in V.J. Barclay, C.E. Dateo, I.P. Hamilton, B. Kendrick, R.T Pack, D.W. Schwenke, *J. Chem. Phys.* **103**, 3864 (1995).

[30] M.R. Pastrana, L.A.M. Quintales, J. Brandão, and A.J.C. Varandas, *J. Phys. Chem.* **94**, 8073 (1990).

[31] (a) R. T. Pack, *J. Chem. Phys.* **60**, 633 (1974). (b) P. McGuire and D. J. Kouri, *J. Chem. Phys.* **60**, 2488 (1974).

[32] C.H. Townes and A.L. Schawlow, *Microwave Spectroscopy* (McGraw-Hill, New York, 1955).

[33] D. Herschbach, *Adv. Chem. Phys.* **10** 319 (1966).

[34] C. W. McCurdy and W. H. Miller, *ACS Symp. Ser. No. 56*, edited by P. R. Brooks and E. F. Hayes (American Chemical Society, Washington, D.C., 1977), pp. 239-242.

[35] H. Diehl, S. Flügge, U. Schröder, A. Völkel, A. Weiguny, *Z. Physik* **162**, 1 (1961).

[36] (a) J.M. Bowman, *Chem. Phys. Lett.* **217**, 36 (1994). (b) J. Qi and J.M. Bowman, *J. Phys. Chem.* **100**, 15165 (1996). (c) J. Qi and J.M. Bowman, *J. Chem. Phys.* **107**, 9960 (1997).

[37] (a) K.H. Kramer and R.B. Bernstein, *J. Chem. Phys.* **40**, 200 (1964). (b) K.H. Kramer and R.B. Bernstein, *J. Chem. Phys.* **44**, 4473 (1966).

[38] D. Wang and J. M. Bowman, *J. Phys. Chem.* **98**, 7994 (1994).

[39] (a) J. Qi and J.M. Bowman, *J. Chem. Phys.* **105**, 9884 (1996). (b) J. Qi and J.M. Bowman, *Chem. Phys. Lett.* **276**, 371 (1997).

[40] B. Kendrick and R.T. Pack, *J. Chem. Phys.* **102**, 1994 (1995)

[41] M.J. Howard and I.W.M. Smith, *J. Chem. Soc. Faraday Trans. 2* **77**, 997 (1981).

[42] N. Cohen, and K.R. Westberg, *J. Phys. Chem. Ref. Data* **12**, 531 (1983).

[43] K.H. Eberius, K. Hoyermann, and H.G. Wagner, *Thirteenth Symposium (International) on Combustion* (The Combustion Institute, Pittsburgh, 1971).

[44] W.H. Miller, *J. Chem. Phys.* **53**, 3578 (1970).

[45] W.H. Miller and T.F. George, *J. Chem. Phys.* **56**, 5668 (1972), Appendix D.

[46] E.J. Heller, *J. Chem. Phys.* **94**, 2723 (1991).

[47] W.H. Miller, *J. Chem. Phys.* **95**, 9428 (1991).

[48] E.J. Heller, *J. Chem. Phys.* **94**, 9431 (1991).

[49] M.A. Sepulveda, S. Tomsovic, and E.J. Heller, *Phys. Rev. Lett.* **69**, 402 (1992).

[50] N.T. Maitra and E.J. Heller, *Phys. Rev. Lett.* **78**, 3035 (1997).

[51] M.F. Herman and E. Kluk *Chem. Phys.* **91**, 27 (1984),

[52] M.F. Herman, *Chem. Phys. Lett.* **275**, 445 (1997),

[53] D. Provost and P. Brummer, *Phys. Rev. Lett.* **74**, 250 (1995),

[54] G. Campolieti and P. Brummer, *Phys. Rev. A* **50**, 997 (1994),

[55] K.G. Kay, *J. Chem. Phys.* **100**, 4377 (1994).

[93] D.A. Micha, *Chem. Phys. Lett.* , **81**, 517 (1981).

[94] D.A. Micha, *J. Chem. Phys.* , **74**, 2054, (1981).

[95] D.A. Micha and E.F. Vilallonga, *J. Chem. Phys.* , **78**, 3942, (1983).

[96] E.F. Vilallonga and D.A. Micha, *J. Chem. Phys.* , **79**, 3794, (1983).

[97] E.F. Vilallonga and D.A. Micha, *J. Chem. Phys.* , **86**, 760, (1987).

[98] E.F. Vilallonga and D.A. Micha, *J. Chem. Phys.* , **86**, 750, (1987).

[99] E.J. Heller, J.R. Reimers, G. Drolshagen, *Phys. Rev. A* , **36**, 2613, (1987).

[100] G. Drolshagen and E.J. Heller, *Chem. Phys. Lett.* , **104**, 129, (1984).

[101] G. Drolshagen and E.J. Heller, *J. Chem. Phys.* , **82**, 226, (1985).

[102] W.H. Miller, *J. Chem. Phys.* **53**, 3578 (1970).

[103] W.H. Miller and T.F. George, *J. Chem. Phys.* **56**, 5668 (1972), Appendix D.

[104] S. Keshavamurthy and W.H. Miller, *Chem. Phys. Lett.* **218**, 189 (1994),

[105] B.W. Spath and W.H. Miller, *Chem. Phys. Lett.* **262**, 486 (1996),

[106] X. Sun H. Wang, and W.H. Miller, *J. Chem. Phys.* **106**, 6346 (1997).

[107] X. Sun and W.H. Miller, *J. Chem. Phys.* **108**, 8870 (1998).

[108] H. Wang, X. Sun, and W.H. Miller, *J. Chem. Phys.* **108**, 9726 (1998).

[109] X. Sun, H. Wang, and W.H. Miller, *J. Chem. Phys.* , **109**, 4190 (1998).

[110] X. Sun, H. Wang, and W.H. Miller, *J. Chem. Phys.* , **109**, 7064 (1998).

[111] D.E. Skinner and W.H. Miller *Chem. Phys. Lett.* **300**, 20 (1998),

[112] V. Guallar, V.S. Batista, and W.H. Miller, *J. Chem. Phys.* **110**, 9922 (1999).

[113] H. Wang, X.Song, D. Chandler, and W. H. Miller, *J. Chem. Phys.* , **110**, 4828, 1998.

[114] V.S. Batista, M.T. Zanni, B. Greenblatt, D.M. Neumark, and W.H. Miller , *J. Chem. Phys.* , **110**, 3736, 1998.

[115] H. Wang, M. Thoss, W. H. Miller, *J. Chem. Phys.* , **112**,47 , 2000.

[116] W. H. Miller, *J. Phys. Chem.* , **103**, 9384 ,(1999).

[117] D. E. Skinner and W. H. Miller*J. Chem. Phys.* , **111**, 10787 ,(2000).

[118] *J. Chem. Phys.* , , ,(1999).

[119] *J. Chem. Phys.* , , ,(1999).

[120] K. Husimi, *Proc. Phys. Math. Soc. Japn.* **22**, 264 (1940).

[121] J.H. Van Vleck, *Proc. Natl. Acad. Sci.* **14**, 178 (1928).

[122] (a) F. Matzkies and U. Manthe, *J. Chem. Phys.* **108**, 4828 (1998). (b) F. Matzkies and U. Manthe, *J. Chem. Phys.* **106**, 2946 (1997).

[123] M.J. Baines, *Moving Finite Elements*; (Oxford U.P., Oxford, 1994).

[124] W.H. Press, S.A. Teukolsky, W.T. Vetterling, B.P. Flannery, *Numerical Recipes in C*; (Cambridge U.P., Cambridge, 1992) Chapter 13.

[125] T.A. Arias, *Rev. Mod. Phys.* **71**, 267 (1999).

[126] Y. Elran, K. G. Kay, *J. Chem. Phys.* **110**, 3653 (1999).

[127] Y. Elran, K. G. Kay, *J. Chem. Phys.* **110**, 8192 (1999).

[128] U. Manthe, unpublished results (2000).

[129] J. A. Jones, M. Mosca, *J. Chem. Phys.* **109**, 1648 (1998).

Ernest Orlando Lawrence Berkeley National Laboratory
One Cyclotron Road | Berkeley, California 94720

Prepared for the U.S. Department of Energy under Contract No. DE-AC03-76SF00098